JOURNAL OF PETROLOGY | VOLUME 49 | NUMBER 9 | PAGES 1667–1686 | 2008 | doi:10.1093/petrology/egn042

Glaucophane-bearing Marbles on Syros, Greece

JOHN C. SCHUMACHER[1]*, JOHN B. BRADY[2], JOHN T. CHENEY[3] AND ROBERT R. TONNSEN[4†]

[1]DEPARTMENT OF EARTH SCIENCES, UNIVERSITY OF BRISTOL, WILLS MEMORIAL BUILDING, BRISTOL BS8 1RJ, UK

[2]DEPARTMENT OF GEOLOGY, SMITH COLLEGE, NORTHAMPTON, MA 01063, USA

[3]DEPARTMENT OF GEOLOGY, AMHERST COLLEGE, AMHERST, MA 01002, USA

[4]GEOLOGY DEPARTMENT, WHITMAN COLLEGE, WALLA WALLA, WA 99362, USA

RECEIVED APRIL 17, 2006; ACCEPTED AUGUST 19, 2008
ADVANCE ACCESS PUBLICATION SEPTEMBER 4, 2008

The occurrence of glaucophane-bearing marbles on Syros is noteworthy because reports of marbles that contain glaucophane are rare among descriptions of high-pressure marbles. On Syros, the marbles are composed primarily of calcite with or without dolomite and quartz. Much of the calcite in these marbles shows oriented columnar structures that are interpreted as pseudomorphs of prismatic aragonite. The columnar structure is particularly well developed in layers of pure $CaCO_3$ and is one indicator of the high-pressure history of these marbles. Metamorphosed admixtures of carbonate and mafic silicate material yielded minerals that are typical for eclogite facies and blueschist facies. These impure marbles are widespread and contain assemblages of various combinations of glaucophane/ferroglaucophane, Na-pyroxene (omphacite to jadeite), epidote, garnet, paragonite and phengitic white mica. Based on calculated mineral equilibria, the assemblages and mineral compositions in the marbles and associated rocks place narrow constraints on the metamorphic P–T *path and the grain-boundary fluid composition of the marbles. The occurrence of glaucophane + $CaCO_3$ + dolomite + quartz suggests that the* P–T *trajectory that was followed by the rocks crossed a reaction such as albite/Na-pyroxene + dolomite + quartz → glaucophane + $CaCO_3$, but did not exceed the* P–T *stability of the reaction dolomite + quartz → tremolite + $CaCO_3$. The* P–T *locations of these reactions are sensitive to fluid composition and indicate that the attending fluid phase was water-rich with X_{CO_2} constrained to be < 0·03; a value of X_{CO_2} of 0·01 best fits the observed assemblages. Relict lawsonite + Al-rich epidote in schists associated with the glaucophane marbles also has a* T–X_{CO_2} *stability that is limited to fluids with X_{CO_2} < 0·03. This observation suggests that the grain-boundary fluid of the whole subduction package of schist, blueschist and marble was rich in H_2O over most of its metamorphic history. The* P–T–X_{CO_2} *stability of assemblages common in the schist and marble constrains the* P *and* T *maxima for these rocks to about 500°C and 15–16 kbar. These* P–T *constraints, together with the tectonic fabric of the marbles, suggest that deformation and recrystallization occurred at or near the thermal maximum of metamorphism.*

KEY WORDS: *glaucophane; marble; Cyclades; Syros; metamorphic petrology*

INTRODUCTION

Amphibole (tremolite, actinolite or hornblende) is a common mineral formed during the prograde metamorphism of impure limestone at low to medium pressure. In the metamorphic rocks of Syros, Greece (Fig. 1), amphibole is present in the marbles, but is glaucophane instead of calcic amphibole. Petrographic descriptions of marbles from high-pressure terrains are uncommon in the geological literature (Castelli, 1991; Wang & Liou, 1993; Ballèvre & Lagabrielle, 1994; Ye & Hirajima, 1996; Boundy *et al.*, 2002), and among these few examples of high-pressure marbles, those marbles that bear prograde glaucophane (Ballèvre & Lagabrielle, 1994) are even more unusual. Ballèvre & Lagabrielle (1994) reported the only prograde glaucophane-bearing marbles from the Alps, and this is the only other example of prograde glaucophane in marble of which we are aware.

Here, we give an overview of the geology of Syros and the timing and conditions of metamorphism, and examine the *P–T–X* conditions under which glaucophane can be stable in marble. Our work suggests that water-rich fluids are essential to stabilizing glaucophane + calcium

*Corresponding author. Telephone: 44-117-954-5417. Fax: 44-117-925-3385. E-mail: j.c.schumacher@bristol.ac.uk
†Present address: Colorado School of Mines, Golden, CO 80401, USA.

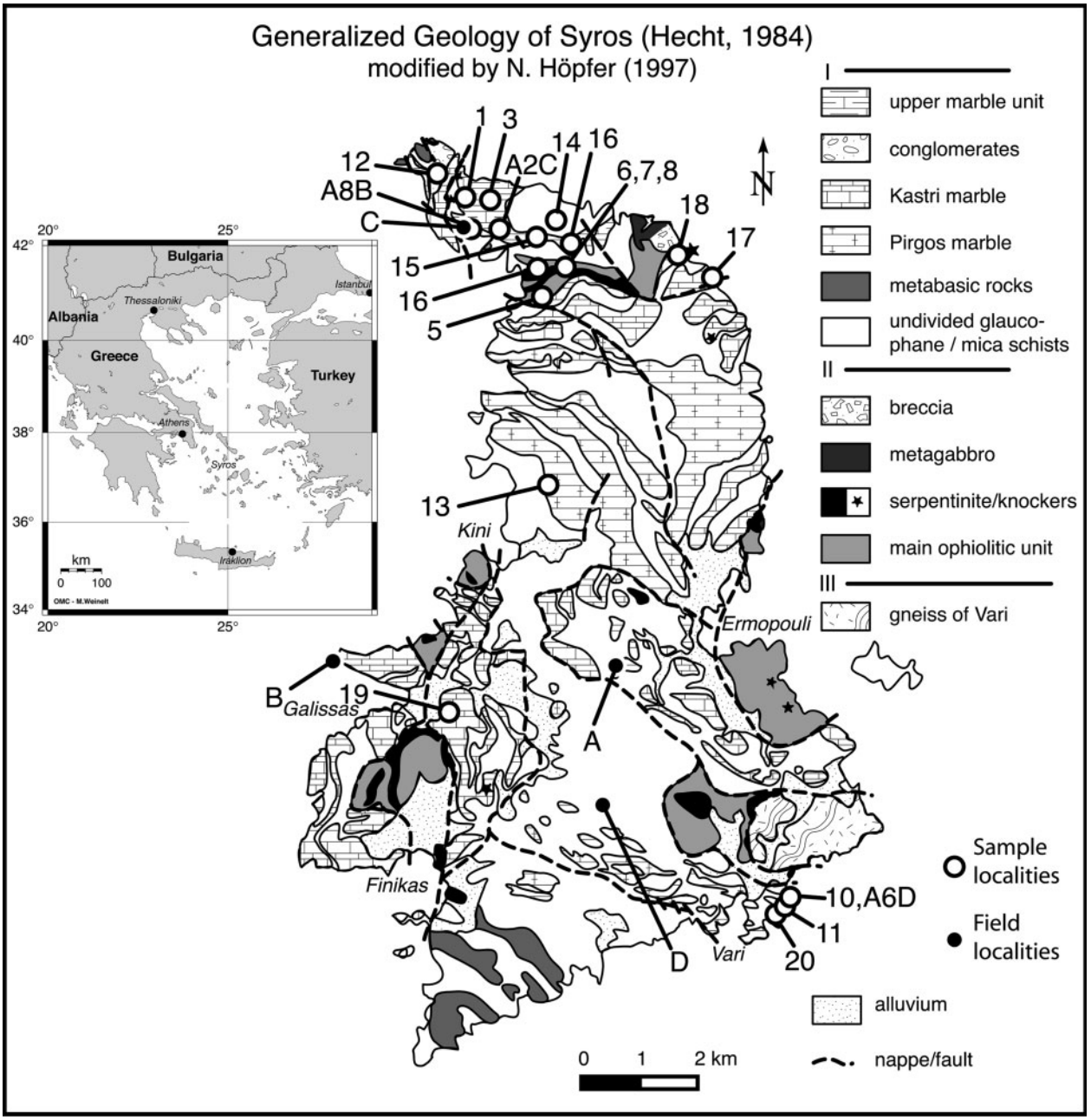

Fig. 1. Generalized geological map of Syros after Hecht (1984) and modified by Höpfer (1997). Inset shows the location of Syros, about 130 km SE of Athens. Numbers indicate sample locations.

carbonate, and we also show that similar water-rich fluids were likely to be present in the schists intercalated with the marbles. The P–T constraints imposed by the presence of glaucophane and the textures in the marbles contribute to understanding the P–T and deformation history of these high-pressure rocks. These interpretive aspects are also discussed with reference to recent contributions in the literature on pressure and temperature trajectories, and the timing of deformation and metamorphism in this part of the Aegean.

GEOLOGICAL SETTING

Tectono-stratigraphy

The rocks of the island of Syros are part of the Attic–Cycladic blueschist belt, which formed during Eurasia–Africa subduction that began in the Mesozoic. The rocks of Syros, as understood at present, can be broadly divided into three tectono-stratigraphic units: (I) metamorphosed sedimentary and volcanic rocks; (II) remnants of oceanic crust consisting of several discrete, fault-bounded packages

of blueschist- or eclogite-facies mafic rocks that contain minor serpentinite; (III) the Vari gneiss, which is a tectonic klippe (Tomaschek & Ballhaus, 1999). With the exception of the Vari gneiss in the SE, the rocks contain high-pressure mineral assemblages reflecting conditions of at least 15 kbar and about 500°C (Dixon & Ridley, 1987; Okrusch & Bröcker, 1990). Unit I is a sequence of volcano-sedimentary rock types (schists and marble in Fig. 1). The lowermost rocks of Unit I that are exposed in the southern part of the island consist of metamorphosed felsic tuffs that may contain felsic clasts, mafic schists, minor marbles, and finely laminated manganese cherts. These rocks give way upwards to a section dominated by marble. The two main lower marble horizons are typically dolomitic, in part, and are separated by intercalated glaucophane schists, epidote–white mica schists, greenschists (retrograde), and minor quartzites and manganese cherts. Apart from carbonates and quartz, the assemblages contain various combinations of glaucophane/ferroglaucophane, Na-pyroxene (omphacite–jadeite), epidote, garnet, paragonite and phengitic white mica. At many marble localities, thin layers bearing silicate minerals define the foliation in the marbles.

N. Höpfer (personal communication, 1997) subdivided the marbles on Syros into two subunits (Pirgos and Kastri Marbles) based on their mineralogy and associated rock types (Fig. 1). The lower Pirgos marble is typically dolomitic and is intercalated with glaucophane-schists, greenschists (retrograde), minor quartzites and minor garnet (fine-grained)–glaucophane to ferroglaucophane-mica schists. Above these marbles, metaquartzites and mafic and mica schists with manganese cherts (coticules) are present. Higher in the section, Kastri Marble horizons are intercalated with glaucophane schists. The Kastri Marble is typically less dolomitic than the Pirgos Marble. Pohl (1999) recognized possible fossils in the Pirgos marble unit north of Ermopouli. D. Vachard & M. Montenari (personal communication, 1999, cited by Pohl, 1999) later confirmed that these features were (microfossil) forams (Family Forschiidae), which are consistent with a Late Tournaisian (Ivorian) to Viséan (330–350 Ma) depositional age.

All of the rocks, except for the interiors of metagabbro in Unit II and locally protected parts of breccia units, are intensely deformed. Small-scale asymmetrical folding features indicate shortening of the entire metamorphic pile containing the blueschist unit during thrusting related to a major collisional event, possibly linked to tectonism on mainland Turkey (Ridley, 1984*b*). A penetrative, metamorphic foliation that is parallel to compositional layering contains the aligned blueschist-facies minerals, which formed during the high-pressure metamorphism (Ridley, 1981, 1982*b*, 1984*b*). Outcrop-scale tight to isoclinal folding with fold axes oriented NE–SW also developed at this stage. The main deformation and fabric-forming event was called D_2 by both Rosenbaum *et al.* (2002) and Keiter *et al.* (2004). Relicts of an earlier D_1 phase include remnants of interfolial folds (Keiter *et al.*, 2004) and rotated S_1 fabrics in garnets (Rosenbaum *et al.*, 2002). Rosenbaum *et al.* (2002) proposed that D_1 occurred at and D_2 just after peak metamorphism, whereas Keiter *et al.* (2004) placed D_1 and D_2 before peak metamorphism. Trotet *et al.* (2001*b*) suggested that the main fabric-forming event coincided with peak metamorphism.

The high-pressure, metamorphic stretching lineation (D_2) trends NE–SW, with top-to-the-NE shear sense, according to Trotet *et al.* (2001*a*). In contrast, based on work in northernmost Syros, both Rosenbaum *et al.* (2002) and Keiter *et al.* (2004) indicated that the lineation associated with the main metamorphic fabric trends NW–SE with top-to-the-SSW shear sense (see also Ridley, 1984*b*, 1986). Later deformation occurs mostly at or near greenschist-facies conditions, and the style of this deformation includes up to kilometer-scale, upright open folds that generally lack an associated schistosity, crenulations and kink bands, all of which deform the D_2 fabrics (see also Rosenbaum *et al.*, 2002; Keiter *et al.*, 2004; and references therein). The youngest deformation is brittle, characterized by normal and listric faults (Ridley, 1984*c*) and local chevron-style folding.

Metamorphism and timing of events

Low-temperature, high-pressure mineral assemblages are found on several islands in the Cyclades (Ridley, 1984*a*, 1984*b*). The best preserved of these rocks are on Syros and Sifnos. Mineral compositions and peak metamorphic assemblages are similar on both islands, and many workers consider both islands to share similar P–T histories. However, constraining the P–T histories of Syros and Sifnos is a work in progress with many contributors. The high-pressure assemblages in this part of the Cyclades all show a later greenschist-facies overprint of varying local intensity and duration.

For Syros, Dixon (1976) suggested peak P–T conditions of 450–500°C and at least 14 kbar based on the occurrence of jadeite + quartz, zoisite + paragonite + quartz and lawsonite together with the absence of lawsonite + jadeite. Ridley (1984*a*, fig. 2) showed that the stability of paragonite also limits the maximum pressure to about 20 kbar at about 575°C. Most reports have placed the peak of metamorphism on both Syros and Sifnos near 15–16 kbar and 500°C with the upper pressure limit not well constrained (see P–T estimates or P–T paths from Schliestedt, 1986; Dixon & Ridley, 1987; Avigad & Garfunkel, 1989, 1991; Okrusch & Bröcker, 1990; Rosenbaum *et al.*, 2002; Keiter *et al.*, 2004; Putlitz *et al.*, 2005). No clear consensus exists for the P–T paths for Syros and Sifnos, and some paths are clearly indicated as schematic by the researchers (e.g. Rosenbaum *et al.*, 2002; Keiter *et al.*, 2004).

One notable exception to most of the other P–T trajectories is the recent work of Trotet *et al.* (2001*b*), which places

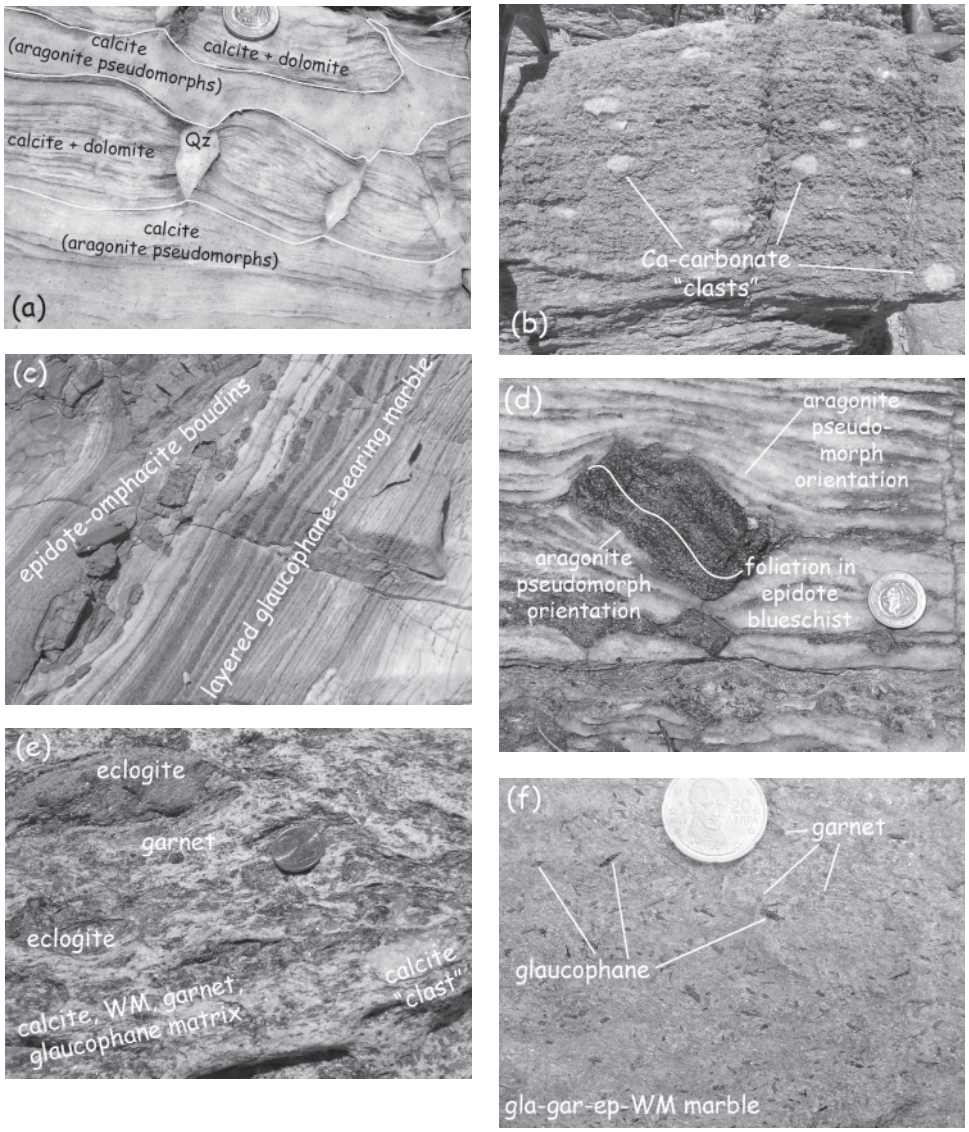

Fig. 2. Outcrop photographs of marble localities. (a) Layers of more massive calcite-rich marble and laminated calcite–dolomite–white mica marble that show ductility contrast (Locality A, Fig. 1); (b) foliated marble with apparent 'clasts' of coarsely grained calcite after aragonite (Locality B, Fig. 1); (c) angular boudinage of epidote–omphacite rock (mafic layers) in impure marble (Locality 6, Fig. 1); (d) rotated, angular boudin of foliated epidote–blueschist in impure marble (Locality C, Fig. 1); (e) eclogite and calcite 'clasts' in glaucophane-bearing marble that contains abundant pseudomorphs after aragonite (Locality 10, Fig. 1); (f) marble bearing coarse glaucophane as well as garnet, epidote and white mica (Locality D, Fig. 1).

the peak metamorphism on Syros at about 19–20 kbar and about 525–550°C based on the TWEEQU approach of Berman (1991). Trotet *et al.* (2001*b*, fig. 9) proposed three different uplift paths for different tectono-stratigraphic locations on Syros (and Sifnos), which is a significant departure from the interpretations of most other workers. Points in time are not correlated on the three P–T paths of Trotet *et al.* (2001*b*), but their proposed existence has significant tectonic implications. Trotet *et al.* (2001*b*, fig. 9b) showed that the rocks present on Syros all experienced the same maximum P–T conditions, but that paths 1 and 2 diverged at the start of uplift (18–19 kbar) and path 3 diverged from path 2 at just below 12 kbar during the uplift phase. Considering the present juxtaposition of the rocks representing these three paths (Trotet *et al.*, 2001*b*, fig. 9b), it is difficult to identify a realistic mechanism that can explain the divergence and reconvergence of these rock units to their present position. Additionally, the P–T conditions of points along these three paths imply the existence of P or T gradients during the uplift phase that seem unreasonable in light of the present stratigraphic thickness, which is about 7·5 km assuming an average dip of 40° ($\Delta P \sim 2{\cdot}15$–$2{\cdot}2$ kbar at an average density of 2·9–3·0).

The geochronology of the Cyclades has been investigated for more than 25 years, but the timing of some events is still debated. The high-pressure metamorphism is widely believed to be Alpine and to have occurred in the Eocene (about 42 Ma). This age is based on Rb–Sr and K–Ar data (Altherr *et al.*, 1979; Anderissen *et al.*, 1979). Recent work (Bröcker & Enders, 1999; Cheney *et al.*, 2000) has suggested that the high-pressure event could be as old as about 80 Ma. However, the interpretation of these ages is not straightforward, and the older ages could also represent either a magmatic age (Tomaschek *et al.*, 2003) or the age of Cretaceous ocean-floor metamorphism. A good summary of the geochronological studies carried out in the region has been given by Putlitz *et al.* (2005). To summarize, the protoliths of the schists and marble units are Paleozoic to Mesozoic in age, and the magmatic rocks of the mafic–ultramafic suite are Cretaceous in age. These units were subducted and metamorphosed to blueschist-facies to lower eclogite-facies conditions at about 50–42 Ma, and the present juxtaposition of units was largely established at the time of peak metamorphism. Partial retrograde metamorphism to greenschist-facies conditions occurred at about 20 Ma (Altherr *et al.*, 1979; Wijbrans *et al.*, 1990; Bröcker *et al.*, 1993). For a more detailed summary of the Cyclades, the reader is referred to Okrusch & Bröcker (1990) and references therein.

PETROGRAPHY AND MINERALOGY

Methods

Spot analyses of minerals in polished thin sections were made using a Cameca SX-100 electron microprobe at 20 kV and 10 nA, with a focused beam, using natural standards, at the University of Bristol. Mineral compositions were also obtained by energy dispersive spectroscopy–scanning electron microscopy (EDS SEM) using a Zeiss DSM 960 instrument, with PGT software for data reduction at Amherst College. Thin sections of the marbles were stained with Alizarin red S to facilitate the identification of dolomite.

Description

The carbonate rocks on Syros can be separated into several general groups: massive marble with indistinct layering of silicate minerals, massive marble with distinct layers of fine-grained dolomite (Fig. 2a), massive marble with distinct layers of silicates, and marbles with conglomerate-like (Fig. 2b) or boudinage textures (Fig. 2c and d). The marbles with distinct layering typically consist of massive marble with layers rich in glaucophane, quartz, and white mica with or without an epidote group mineral, sodic pyroxene, garnet or albitic plagioclase. Marbles with layers of mafic (basaltic) material may show rotation of angular boudinage (Fig. 2d). In the marbles with conglomerate-like textures, 'clasts' generally range between 2 and 8 cm across and are most commonly marble fragments (Fig. 2b); however, eclogite clasts are found in several localities (Fig. 2e). If the carbonate clasts are a relict sedimentary rather than a ductile deformation feature, then they would represent matrix-supported intraclasts (Kenter, 1990). The massive marbles without distinct foliation can contain a variety of minerals including epidote, garnet and white mica dispersed throughout the rock.

Carbonate minerals

Calcite is the major carbonate mineral (Table 1), forming equant to slightly elongate grains that are generally less than 3 mm along the longer axis. Grain boundaries are generally straight, and grain-boundary triple junctions of calcite grains in similar crystallographic orientation show interfacial angles of nearly 120° that suggest textural equilibrium. Single calcite grains may display a slightly undulose extinction and deformation twins are found in most samples. Optically, the calcite grains show small strain-induced 2V angles ($\leq$10°). In layers of relatively pure calcium carbonate, relict boundaries of columnar aragonite are visible in hand specimen; the aragonite, present at high pressures, has been completely replaced by polycrystalline calcite (Brady *et al.*, 2004). The aragonite pseudomorphs are common on Syros and have been observed at all the outcrops shown in Fig. 2. Calcite pseudomorphs after aragonite have also been observed on the northern part of Sifnos and are best observed macroscopically, but the texture is also evident in thin section (see Brady *et al.*, 2004, for examples of these textures). No relict aragonite has been identified.

Dolomite is common in impure marbles, and textures suggest that there may be several generations of dolomite, which could result from prograde reactions or retrograde re-equilibration. Dolomite grains are generally less than 3 mm across. In most samples, dolomite is indistinguishable texturally from calcite and was apparent only after staining with Alizarin red S. The dolomite has no consistent relative grain-size relationship with calcite, and, depending upon the sample, dolomite grain size may be either coarser or finer than, or equivalent to, that of the coexisting calcite. In some samples, minor hydration has caused very fine-grained iron oxides or hydroxides to form along cleavage fractures or at grain boundaries (e.g. samples 17B, 11A, 10A, 18), which distinguishes some dolomite grains from the enclosing calcite grains in unstained samples. In sample 16B dolomite is found adjacent to skeletal garnets (Fig. 3a) partially enclosed in calcite. The Mg in dolomite is replaced by about 30% Fe (Fig. 4a).

Glaucophane

The only amphiboles in the marbles are sodic amphiboles. Prisms of glaucophane are generally less than 2 mm in length parallel to the *c*-axis (Figs 2f and 3b, c).

Table 1: Estimated modes and assemblages of marble samples (see Fig. 1)

Sample	cc	qz	dol	gln	Na-cpx	gar	wm	ep	chl	plg	ti	sulfide	ap	oxide
18A	85	4	1	2	1		5	1		<1				
18C	35	1	3	15	35		2	5		1	3			
14A	80	10	4	1	<1		4	1						
11A	60	16	<0·1	3		1	12	5	2					
8A1	90	1	0·5	4		<0·1			0·5	1				
1A	90	2	1	2		<1	3	1						
15	85	3	5	2			4		1	<1				
A2C*	80	5	4·5	3			4	3	<1					
12F	85	5	2	<0·1			1		1·5	5				
A6D*	68	5	2	4		4	15	1						
17B	65	3	25				6							<1
10B	60	34	2				4							
10A	50	45	3				2							
11D	55	20		8		1	10							
16A	93	3		1		2	1							
13B	55	15		<1		<1	5	<1		20				
5A	95	0·1		0·5			1·8	0·2	0·2	0·2				
5B	88	<0·3		3			6			1				
3C	93	0·2		<1			2	<1						
3B	70	5			9		6	6			1	1		
A8B*	88	3			4		3	2						
12A	90	5					3		1	1				
12D	80	9					4		1	6				<1
6A	85		1	1	5		2	1	4				0·1	
16B	40		3	1	20	6	30	<1	<1	<1				
7B	85		<1		5	6	2		2					
19A	15		75				10							
20	15	60				5	20							

*Localities from J.C.S. Other localities are from R.R.T.; locality numbers are in the range of 1–20 and letters or numbers appended to the locality numbers indicate different hand specimens or sawn slabs from that specimen. cc, calcite; qz, quartz; dol, dolomite; gln, glaucophane; Na-cpx, jadeitic to omphacitic pyroxene; gar, garnet; wm, white mica; ep, epidote group mineral; chl, chlorite; plg, albitic plagioclase; ti, titanite; ap, apatite.

The grains have pale blue to nearly colorless pleochroism. According to the nomenclature of Leake *et al.* (1997), compositions lie mostly in the glaucophane field (Fig. 5a) with a few approaching ferroglaucophane. Some glaucophane grains have partial overgrowths of more riebeckitic compositions (more intense blue pleochroism). The stoichiometrically calculated X_{Fe3+} $[Fe^{3+}/(Fe^{3+}+Al)]$ value in most analyses is below 0·15 (Fig. 5b). The glaucophane analyses have very low Ti and Mn, which is less than 0·04 per 23 oxygen formula (Table 2). In most samples, Ca is less than 0·10 per 23 oxygens. In one sample (A2C) that showed Ca zoning, Ca is as high as 0·34 and as low as 0·13 per 23 oxygens (Table 2). Small amounts of Na and very minor K are present at the *A* site (Na + K ≤0·1 per 23 oxygens).

Clinopyroxene

Both the habit and composition of the pyroxenes found in the glaucophane-bearing marbles vary considerably from place to place. The Na- and Na–Ca-clinopyroxenes are commonly prismatic and elongate, and may form aggregates (e.g. Fig. 3d). Cross-sections rarely reach a few millimeters. Their pleochroism is pale apple green to colorless. The compositions of the pyroxenes range from rich in omphacite to very rich in jadeite. The acmite component ($NaFe^{3+}Si_2O_6$) is as high as about 50% in some samples (Fig. 4b). The X_{Mg} of the omphacitic pyroxene is greater than 0·80 (Table 2).

Garnet

Where present, garnet or concentrations of fine-grained garnet are generally less than 3 mm across (Figs 2e, f

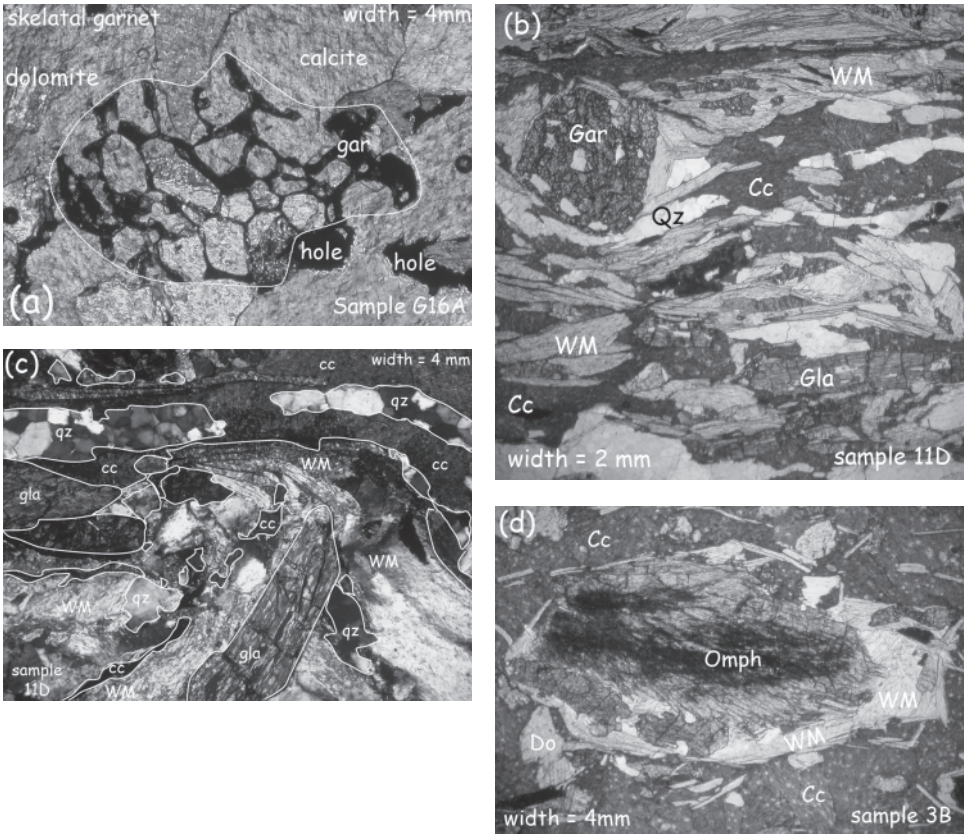

Fig. 3. Photomicrographs of thin sections. (a) Skeletal garnet (Gar) growing at grain boundaries (plane-polarized light; PPL); (b) gar–glaucophane (gla)–white mica (WM) marble (note pressure shadows around the garnet) (PPL); (c) gar–gla–WM marble that shows folding of the main deformational fabric (cross-polarized light; XPL); (d) aggregate of prismatic omphacite with dolomite (Do) and white mica in marble (PPL).

and 3b) and may contain abundant inclusions of colorless minerals such as quartz, calcite and clinozoisite. In some samples (11A, 11D, 16A, 16B, 7B, 8A1, 1A), these inclusion-rich textures grade into skeletal textures (Fig. 3a). In the skeletal textures, garnet nucleated and grew along calcite grain boundaries and formed networks several millimeters across. In hand specimens that contain skeletal garnets, the garnets appears as pale pink patches, but with the aid of a hand lens the inclusion-rich habit of the garnets is evident. The chemical compositions of all garnet types are dominated by the almandine and grossular components with very low pyrope contents (Fig. 6a). Traverses with the electron microprobe (Fig. 6b) show little or no variation in the garnet compositions except for very narrow rims, which commonly show a dramatic increase in spessartine component. In one extreme analysis, the spessartine component is greater than 60% (Table 2). Most of the increase in spessartine is at the expense of the almandine component (Table 2).

White micas

Both phengitic potassium micas and paragonite are found in some of the marbles (e.g. Fig. 3b–d, Table 1). The phengites have up to about 3·4 Si per 11 oxygen p.f.u. The paragonites are close to end-member composition and have very little potassium at the interlayer sites (Table 2). The phengite interlayer sites are occupied by about 80% K and 10–15% Na with vacancies less than 10% (Fig. 4c).

Quartz

Quartz is commonly the second most abundant mineral after carbonates in single samples of the marbles (Table 1). In samples that contain deformation microtextures, quartz aggregates are commonly made up of polygonal grains that appear to replace deformed single grains of quartz that were flattened and stretched during the main deformational episode. The recrystallization of the quartz progressed to differing extents in various samples. In some samples (e.g. Fig. 3c) polycrystalline quartz grains (0·2 mm across) have straight boundaries and show triple junction angles of about 120° that suggest textural equilibrium. Other samples of polycrystalline quartz have irregular, lobate boundaries that suggest arrested recrystallization and coarsening.

Epidote group minerals

Epidote group minerals in the marbles occur most commonly together with garnet, omphacite and glaucophane.

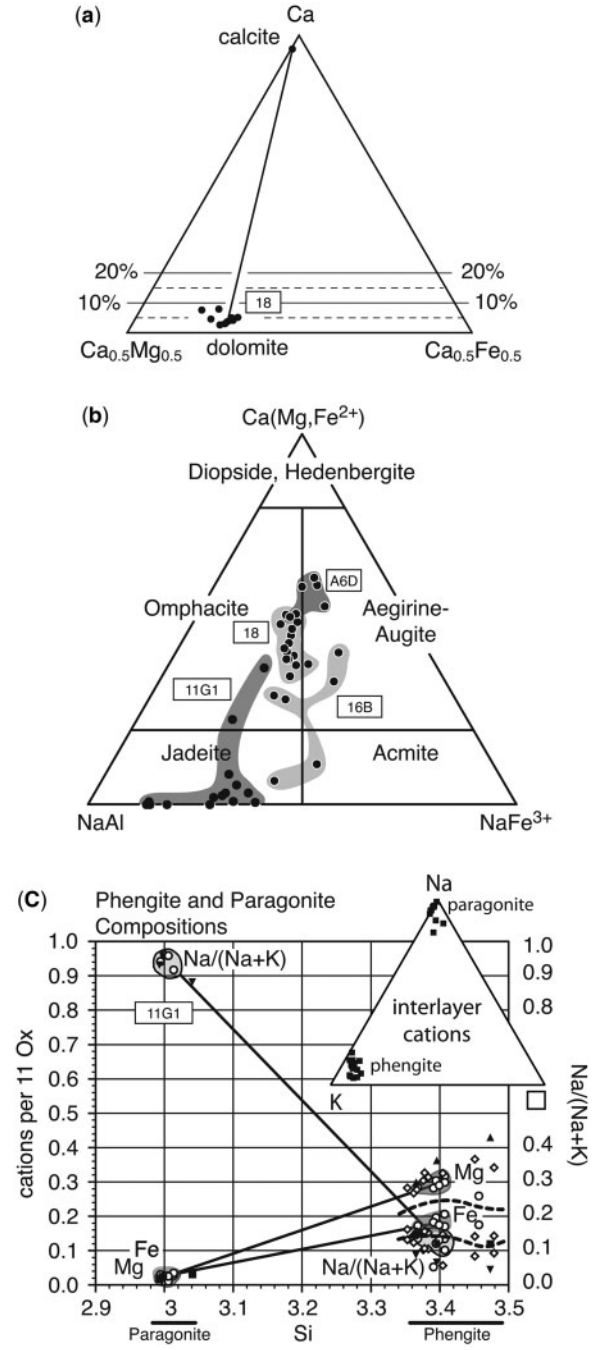

Fig. 4. Plots of mineral compositions. (a) Ca–($Ca_{0·5}Mg_{0·5}$)–($Ca_{0·5}Fe_{0·5}$) ternary showing carbonate mineral composition; (b) pyroxene compositions on a ternary diagram after Morimoto *et al.* (1988); (c) *x*–*y* plot that compares Fe, Mg and Na/(Na + K) in phengite and paragonite. The tie-lines indicate compositions of coexisting white micas. The inset shows the relative proportions of Na, K and vacancy at the interlayer site.

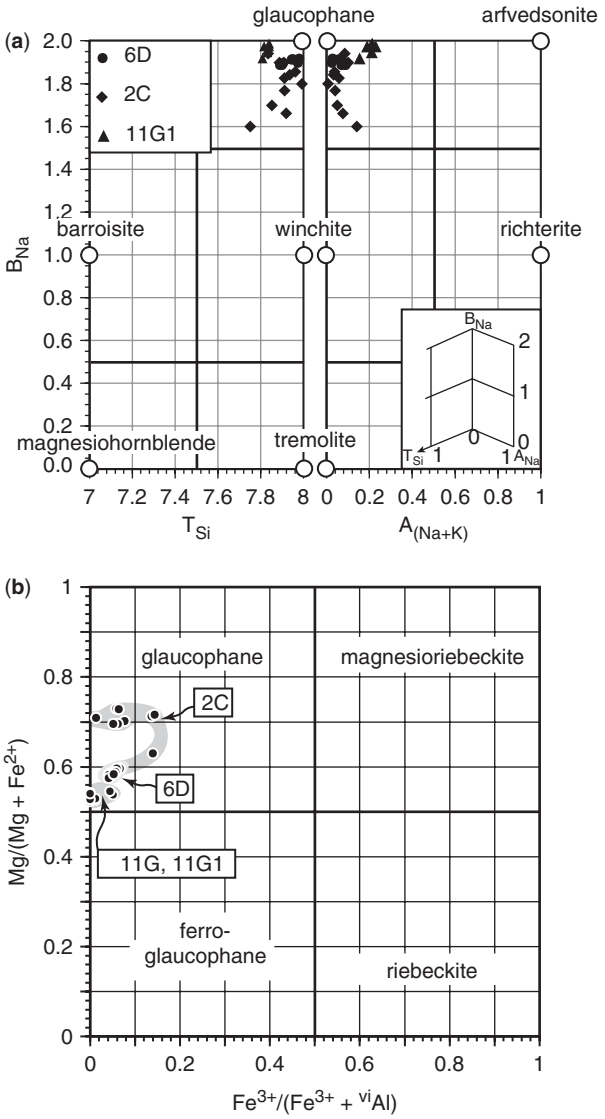

Fig. 5. Glaucophane compositions. (a) Matched plots that show the variation of tetrahedral Si (^{T}Si) vs Na at the B site (^{B}Na) and Na + K at the A site (^{A}Na) for glaucophane (after Leake *et al.* (1997, fig. 1); (b) $Fe^{3+}/(Fe^{3+} + Al^{vi})$ vs $Mg/(Mg + Fe^{2+})$.

In samples that contain both chlorite and albite, epidote either is not present or is only a very minor phase. Individual epidote grains are commonly zoned and compositions in all the samples range between 0·045 (zoisite, orthorhombic; based on optics) and 0·85 Fe^{3+} per 12·5 oxygens, but most compositions lie in the range of 0·4–0·7 Fe^{3+} per 12·5 oxygens and would straddle the clinozoisite–epidote composition fields for a boundary placed at 0·5 Fe^{3+} per 12·5 oxygens.

Albite

Plagioclase, if present in the marbles, is albite (<An_5), and is probably associated with the greenschist-facies overprint. However, in places, anhedral albite in the marbles may partially enclose euhedral glaucophane, which suggests that some albite is not a retrograde phase growing at the expense of glaucophane. The glaucophane + albite may have formed

during local rehydration that occurred during the initial stages of decompression and thus represent a near-peak retrograde metamorphic assemblage

Chlorite

In the marbles, chlorite is found replacing garnet and associated with albite. As a result, the chlorite appears to be associated with the greenschist-facies overprint.

Summary

Variations in the Fe–Mg and Ca contents of the four major Fe–Mg phases in the marbles (clinopyroxene, glaucophane, garnet and dolomite) are summarized in Fig. 7. Pyroxenes and garnets show the most variation in Ca content. The relative X_{Mg} of the Fe–Mg phases is clinopyroxene > dolomite > glaucophane ≫ garnet.

P, *T* AND FLUID COMPOSITIONS

Stability of glaucophane and $CaCO_3$

The assemblages of the glaucophane-bearing marbles place constraints both on the maximum temperatures and pressures, and on the X_{CO_2} of the coexisting fluid in these rocks. The system K_2O–Na_2O–CaO–FeO–MgO–Fe_2O_3–Al_2O_3–SiO_2–H_2O–CO_2 describes the observed mineralogy and compositional variation of the marble assemblages, but a few simplifying assumptions allow the choice of a derivative set of system components and phase components for modelling. Paragonite, phengite, garnet and epidote do not limit the stability of glaucophane + calcium carbonate, and their presence identifies bulk compositions with K_2O and/or $Al/(Na + K) > 1$. In the sense of Korzhinskii (1959), K_2O would be an inert determining component resulting in the presence of phengite, whereas garnet, paragonite and the zoisite component of the epidote mineral are stabilized by Al in excess of that needed to form amphibole and pyroxene phase components.

The system components can be further simplified by ignoring FeO and Fe_2O_3, which are present in the sodic amphibole and clinopyroxene, which allows the system components to be recast as $NaAlO_2$–CaO–MgO–SiO_2–H_2O–CO_2. The initial model (Fig. 8a) uses pyroxene (diopside–jadeite solid solution)–glaucophane–tremolite–albite–dolomite–aragonite–calcite–quartz, which should yield upper pressure stability limits of the assemblages. Although the modelling could be extended to include garnet, paragonite and zoisite, adding these phase does not bear directly on the objective of determining the *P*–*T* stability limits of glaucophane + aragonite/calcite in the marbles. All the additional reactions involving garnet, paragonite and the zoisite + glaucophane and aragonite or calcite are constrained to lie within the part of *P*–*T*–X_{CO_2} space that defines the limits of glaucophane + aragonite/calcite (shaded area in Fig. 8a), because assemblages that limit glaucophane + aragonite/calcite are contained in the six-component system $NaAlO_2$–CaO–MgO–SiO_2–H_2O–CO_2, which is a subset of the seven-component system $NaAlO_2$–CaO–MgO–Al_2O_3–SiO_2–H_2O–CO_2 that is required to add garnet, paragonite

Table 2: Representative mineral analyses of glaucophane, sheet silicates, clinopyroxene and garnet with structural formulae calculated on the anhydrous basis of 23, 11, 6 and 12 oxygens

	Glaucophane			
Sample:	11G	A6D	A2C	A2C
Ferric est.:	13eCNK	15eNK	15eNK	13eCNK
wt %				
SiO_2	57·10	57·85	57·86	55·52
TiO_2	0·07	0·00	0·01	0·08
Al_2O_3	10·63	11·41	11·37	10·30
Cr_2O_3	0·00	0·01	0·00	0·03
FeO	13·07	12·11	9·17	10·28
MnO	0·03	0·08	0·03	0·07
MgO	8·38	8·84	10·76	11·52
CaO	0·39	0·37	0·88	2·23
Na_2O	7·74	7·19	7·04	6·41
K_2O	0·01	0·01	0·01	0·03
Total	97·42	97·85	97·13	96·46
	fixed cations/23 oxygen			
T site				
Si	7·971	7·962	7·920	7·714
Al	0·029	0·038	0·080	0·286
D site				
Al	1·720	1·812	1·755	1·401
Ti	0·007	0·000	0·001	0·008
Cr	0·000	0·001	0·000	0·003
Fe^{3+}	0·081	0·141	0·191	0·470
Mg	0·192	0·046	0·054	0·119
C site				
Mg	1·552	1·767	2·141	2·268
Fe	1·445	1·233	0·858	0·724
Mn	0·003	0·000	0·001	0·008
B site				
Fe	0·000	0·020	0·000	0·000
Mn	0·000	0·009	0·003	0·000
Ca	0·058	0·054	0·128	0·332
Na	1·942	1·918	1·869	1·668
A site				
Na	0·154	0·000	0·000	0·059
K	0·002	0·002	0·002	0·005
Sum	15·156	15·002	15·002	15·142
X_{Mg}	0·546	0·591	0·719	0·767

(continued)

Table 2: Continued

	Par	Par	Phen	Phen	Phen	Phen		Clinopyroxene					Garnet		
Sample:	A6D	A6D	A6D	A2C	A8B	18		A8B	18	11G1	11G1		A6D	16B2	16B2
wt %															
SiO_2	47·06	47·25	49·49	51·15	51·09	49·97		53·66	55·51	58·63	56·96		37·08	37·88	37·44
TiO_2	0·04	0·05	0·16	0·11	0·16	0·32		0·02	0·14	0·18	0·03		0·03	0·05	0·05
Al_2O_3	39·85	38·38	27·86	25·14	24·78	27·29		4·48	12·18	20·79	16·64		21·28	20·66	20·76
Cr_2O_3	0·03	0·03	0·03	0·04	0·03	0·02		0·01	0·03	0·00	0·00		0·04	0·00	0·00
FeO	0·28	0·56	2·48	2·06	2·80	2·73		10·85	7·68	5·00	9·72		27·35	31·80	5·61
MnO	0·00	0·02	0·00	0·01	0·01	0·00		0·04	0·10	0·00	0·05		1·21	1·94	27·74
MgO	0·24	0·40	2·92	4·22	4·09	3·03		8·98	5·34	0·48	0·52		1·64	1·81	0·33
CaO	0·15	0·11	0·10	0·16	0·09	0·07		16·05	8·94	0·54	1·24		11·77	6·71	7·11
Na_2O	7·16	6·54	0·58	0·30	0·26	0·75		5·20	9·42	15·04	14·48		0·00	0·00	0·00
K_2O	0·84	1·38	9·66	10·26	10·10	9·81		0·00	0·06	0·00	0·00		0·00	0·00	0·00
Total	95·64	94·73	93·28	93·45	93·41	94·01		99·30	99·41	100·64	99·64		100·40	100·98	99·70
	cations/11 oxygen							cations/6 oxygen					cations/12 oxygen		
Si	2·994	3·042	3·365	3·473	3·480	3·381	Si	1·974	1·976	1·994	1·990	Si	2·931	3·019	3·037
Al	1·006	0·958	0·635	0·527	0·520	0·619	Al	0·026	0·024	0·006	0·010	Al	0·069	0·000	0·000
Al	1·983	1·954	1·598	1·486	1·469	1·558	Al	0·168	0·486	0·827	0·675	Al	1·914	1·940	1·984
Ti	0·002	0·002	0·008	0·006	0·008	0·016	Ti	0·000	0·004	0·005	0·001	Ti	0·002	0·003	0·003
Cr	0·001	0·002	0·002	0·002	0·002	0·001	Cr	0·000	0·001	0·000	0·000	Cr	0·002	0·000	0·000
Fe^{3+}	0·000	0·000	0·000	0·000	0·000	0·000	Fe^{3+}	0·228	0·182	0·142	0·284	Fe^{3+}	0·151	0·017	0·000
Mg	0·023	0·039	0·296	0·427	0·415	0·306	Mg	0·492	0·283	0·024	0·027	Mg	0·194	0·215	0·040
Fe	0·015	0·030	0·141	0·117	0·159	0·155	Fe	0·106	0·043	0·000	0·000	Fe	1·657	2·102	0·381
Mn	0·000	0·001	0·000	0·001	0·001	0·000	Mn	0·001	0·000	0·001	0·001	Mn	0·081	0·131	1·906
Ca	0·010	0·007	0·007	0·012	0·007	0·005	Mg	0·000	0·000	0·000	0·000	Ca	0·997	0·573	0·618
Na	0·883	0·816	0·077	0·040	0·034	0·099	Fe	0·000	0·003	0·000	0·000				
K	0·068	0·113	0·838	0·888	0·878	0·847	Mn	0·000	0·003	0·000	0·000				
							Ca	0·633	0·341	0·020	0·047				
							Na	0·371	0·650	0·992	0·981				
							K	0·000	0·003	0·000	0·000				
Sum	6·985	6·964	6·967	6·978	6·972	6·987		4·000	4·000	4·010	4·015		8·000	8·000	7·968
X_{Mg}	0·604	0·563	0·677	0·785	0·723	0·664		0·823	0·868	1·000	1·000		0·105	0·093	0·096

Ferric iron in the amphibole was estimated from stoichiometric constraints (see Robinson *et al.*, 1982, pp. 6–10; Leake *et al*. 1997, Appendix I). Ferric iron in the pyroxene was estimated by fixing cations to four (A8B, 18) and assuming all Fe to be ferric in the two compositions from 11G1. Ferric iron in the garnet was estimated by fixing cations to eight. 13eCNK, 13 cations exclusive of Ca, Na and K; 15eNK, 15 cations exclusive of Na and K; par, paragonite; phen, phengite; $X_{Mg} = Mg/(Mg + Fe^{2+})$.

and zoisite. Additionally, adding pyrope to the modelling would be of questionable value because, unlike the other Fe–Mg silicates, the Mg end-member content of the real garnet compositions is practically non-existent. Nevertheless, the effects of adding FeO and Fe_2O_3 need to be addressed.

Figures 4 and 7 show that X_{Fe2+} is about 0·3–0·5, but X_{Fe3+} less than 0·1 in the sodic amphibole, whereas X_{Fe2+} is less than 0·1, but X_{Fe3+} is around 0·3–0·5 in the sodic pyroxene. In general, substitution of Fe^{2+} in Fe–Mg silicates lowers their thermal stability; modelling the P–T stability of reactions that limit glaucophane + aragonite/calcite from Fig. 8a indicates that addition of FeO will slightly reduce the assemblage's maximum T, but that the maximum P falls several kilobars and the assemblage's stability shrinks drastically (Fig. 8b). Similarly, adding FeO reduces the T–X_{CO_2} range of conditions for the stable assemblage sodic amphibole + aragonite/calcite (Fig. 8c).

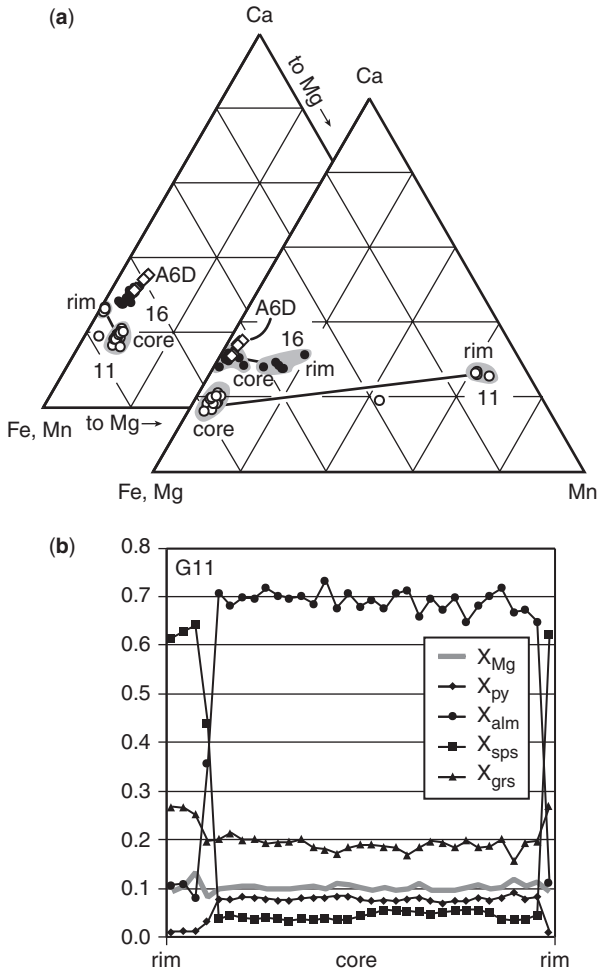

Fig. 6. (a) Ternary plots of garnet compositions showing the relative proportions of (Fe + Mn)–Ca–Mg and (Fe + Mg)–Ca–Mn; (b) a compositional profile across one garnet (G11) for Ca, Mn, Fe and Mg, and X_{Mg} [= Mg/(Mg + Fe^{2+})].

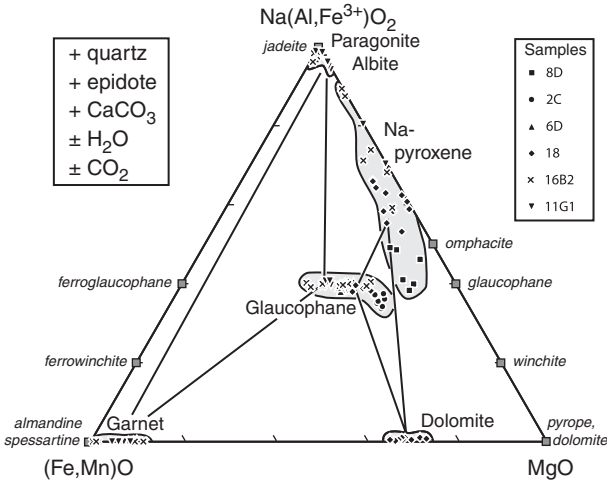

Fig. 7. Comparison of the relative Fe–Mg contents of the major Fe–Mg-bearing phases on a projection from quartz, epidote, calcite, H_2O and CO_2 onto the $Na(Al, Fe^{3+})O_2$–(Fe, Mn)O–MgO plane. It should be noted that this is not strictly a thermodynamically valid projection, because of $Al + Fe^{3+}$ and FeO + MnO being combined. Coordinates are $Na(Al, Fe^{3+})O_2 = 2\ Na_2O$, (Fe, Mn) O = FeO + MnO, MgO = MgO.

Modelling reactions to include both FeO and Fe_2O_3 has the benefit of making the system a much closer analog of the observed one; the disadvantage is that the estimates of thermodynamic properties and the activities that incorporate ferric end-members of Fe–Mg silicates are not as well tested. We explored the effects of both FeO and Fe_2O_3 with one reaction, glaucophane + aragonite = $omphacite_{ss}$, using the most recent version (HP02) of the data from Holland & Powell (1998) and the activity models of Holland & Powell (1996) and Dale *et al.* (2000) as implemented in Perplex.07 (Connolly, 1990, 2005) for the amphibole end-members glaucophane, ferroglaucophane, magnesioriebeckite and riebeckite and the pyroxene end-members diopside, hedenbergite, jadeite and acmite. For glaucophane compositions with $X_{Mg} = 0{\cdot}7$–$0{\cdot}5$ and $X_{Fe3+} = 0{\cdot}0$–$0{\cdot}1$, which closely match the range of measured compositions from this study, the stable breakdown reactions for sodic amphibole + aragonite/calcite for the entire range of glaucophane compositions closely coincide and lie about 25° below the Mg end-member reaction (iii in Fig. 8a). As a consequence, modeling the P–T–X_{CO_2} stability of glaucophane + aragonite/calcite as Mg end-members, which considerably simplifies the calculation and analysis of the phase equilibria, would reasonably appear to represent the conditions of stability of sodic amphibole + aragonite/calcite on Syros and overestimate temperatures by no more than about 25°C, which is well within the uncertainty of most P–T estimates.

Phase relations in the system $NaAlO_2$–CaO–MgO–SiO_2–H_2O–CO_2 indicate that no stability field for glaucophane plus aragonite/calcite exists at X_{CO_2} values slightly above about 0·03. Figure 8a shows the phase relations at $X_{CO_2} = 0{\cdot}01$, and the shaded area in the center of the figure shows the limits of glaucophane + aragonite/calcite. Based on the assemblages reported in this study, the important prograde reactions that form glaucophane marbles are albite + dolomite = glaucophane + aragonite/calcite and jadeite-rich clinopyroxene + dolomite = glaucophane + aragonite/calcite (i and ii in Fig. 8a). Ideally, the upper thermal stability limits of the glaucophane marbles are continuous reactions: glaucophane + 3 aragonite/calcite + 2 quartz = $omphacite_{ss}$ (e.g. $Jd_{40}Di_{60}$) + fluid (1 H_2O + 3 CO_2) and 5 glaucophane + 8 quartz + 22 aragonite/calcite = $omphacite_{ss}$ (e.g. $Jd_{50}Di_{50}$) + fluid (4 H_2O + 22 CO_2) + tremolite (iii and iv in Fig. 8a).

Isopleths that are estimates of the diopside contents of the associated clinopyroxenes and assemblage information are also given in Fig. 8a. It is also worth noting that for reactions involving glaucophane, aragonite and Na–Ca

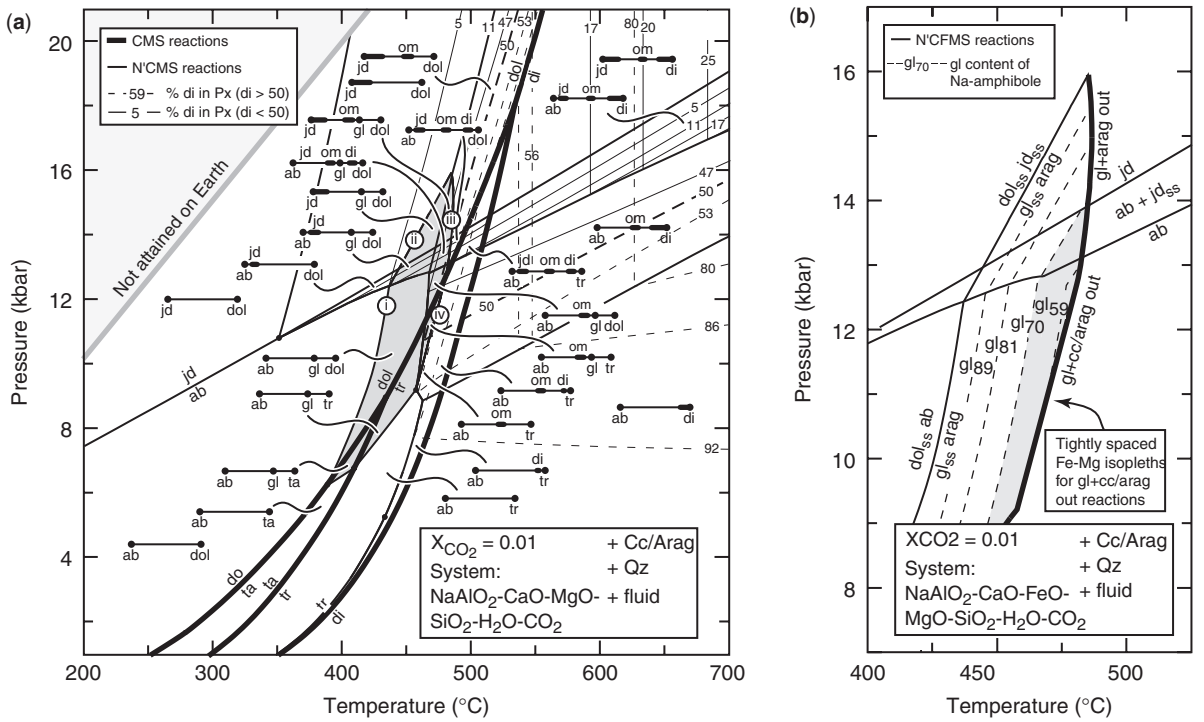

Fig. 8. Pressure vs temperature and temperature vs X_{CO_2} diagrams. (a) reactions in the system $NaAlO_2$–CaO–MgO–SiO_2–H_2O–CO_2 among the phases dolomite (dol), tremolite (tr), talc (ta), albite (ab), jadeite (jd), diopside (di), omphacite (om) and glaucophane (gl) with quartz (qz), calcite (cc) and aragonite (arag) present as excess phases. The gray field is the stability field of gl + arag/cc. The lower-case Roman numerals indicate reactions that bound the parts of the stability field of glaucophane + $CaCO_3$ relevant to this study: (i) ab + dol = gl + arag/cc; (ii) jd-rich clinopyroxene + dol = gl + arag/cc; (iii) gla + arag/cc = om; (iv) gl + arag/cc = om + tr. Fine dashed and continuous lines are compositional isopleths for jd–di solid solution: fine continuous lines represent isopleths for pyroxenes with jd component > 50% and fine dashed lines are isopleths for pyroxenes with di component > 50%. On this diagram, the isopleth for the composition of ideal omphacite ($Jd_{50}Di_{50}$) is dashed and, for emphasis, drawn thicker than the other isopleths. The stable Na–Ca pyroxenes may be jd-rich, omphacitic or di-rich; compositional phase for each field indicates the ranges of pyroxene compositions that may be present. (b) Reactions in the system $NaAlO_2$–CaO–FeO–MgO–SiO_2–H_2O–CO_2 that show Fe reduces the P–T stability field of calcite/aragonite + glaucophane; gl_{ss}, glaucophane Fe–Mg solid solution; jd_{ss}, Ca–Na–Fe–Mg solid solution in Na-rich pyroxene. (c) Reactions in the system $NaAlO_2$–CaO–FeO–MgO–SiO_2–H_2O–CO_2 at 15 kbar that show Fe reduces the T–X_{CO_2} stability field of calcite/aragonite + glaucophane. Calculations were carried out with PerPlex (Connolly, 1990, 2005) using the HP02 thermodynamic data of Holland & Powell (1998). Solid solution models: dolomite–ankerite (Holland & Powell, 1998), Na–Ca pyroxene solid solution (Holland & Powell, 1996) and a Margules-type glaucophane–ferroglaucophane model as implemented in PerPlex (see documentation at http://www.perplex.ethz.ch/).

pyroxene the model predicts extensive variations in pyroxene composition with relative small variations in P–T (see closely spaced compositional isopleths in Fig. 8a). Zoning would be expected in the natural samples, and this agrees well with the observed Na–Ca pyroxenes, which show variations in Na/(Na + Ca) up to 0·35–0·40 (Fig. 4b).

The upper temperature and pressure limits of glaucophane + aragonite are at about 480–485°C and 15–16 kbar. The effects of adding FeO to the estimates are shown in Fig. 8b. Essentially, Fe has little discernible effect on the upper temperature stability, where the isopleths for variable Fe in glaucophane and omphacite are tightly clustered; however, adding Fe moves the lower stability limit to higher temperatures, and shrinks the range of pressure and temperature over which glaucophane + aragonite/calcite is stable.

Other calculations were carried out at $X_{CO_2} = 0{\cdot}005$, 0·020 and 0·030 in the Mg end-member system to establish the extent of the P–T stability of glaucophane + calcium carbonate. Together these define a P–T region for glaucophane + aragonite and indicate that at values slightly above $X_{CO_2} = 0{\cdot}03$ glaucophane is no longer stable in marble (Fig. 9). The maximum glaucophane + aragonite P–T stability is marked by a steep (*c.* 140 bar/°C), negatively sloping curve that is concave to lower T and along which X_{CO_2} varies (Fig. 9), with the maximum possible temperature just above 515°C and about 11–11·2 kbar.

The glaucophane-bearing marbles from the Queyras unit in the Western Alps (Ballèvre & Lagabrielle, 1994) share some features with those of Syros. The Queyras assemblages are calcite + quartz + garnet ± glaucophane (in two samples) ± phengite ± chlorite ± titanite ± lawsonite (one pseudomorph, now zoisite + phengite) and are subsets of assemblages found on Syros. Noteworthy differences between the Queyras and Syros glaucophane-bearing marbles are the lack of Na-pyroxene and paragonite in the Queyras marbles. The compositions of

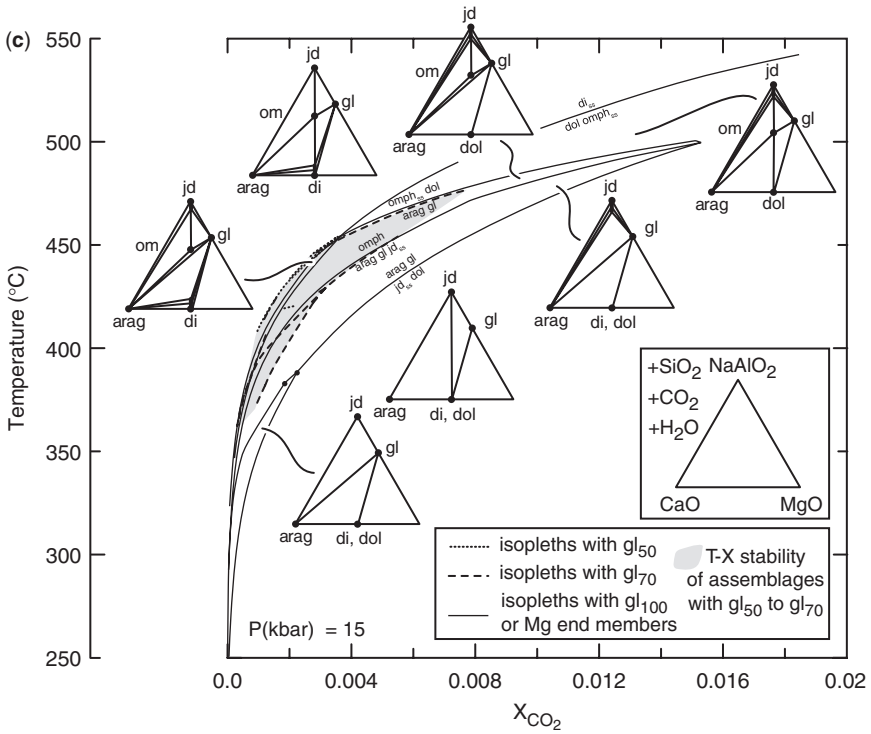

Fig. 8. Continued.

glaucophane and garnet from the glaucophane-bearing marbles from both Queyras and Syros are similar; however, garnet from Syros, although low in pyrope component (3–10 mol %), is richer in pyrope that those from the Queyras unit (≤1 mol %). Ballèvre & Lagabrielle (1994) reported that the estimated metamorphic conditions for the Queyras glaucophane marbles are 10 kbar and 400°C (Nitsch, 1972; Kerrick & Jacobs, 1981; Frey, 1987). Ballèvre & Lagabrielle (1994) also suggested that the attending fluid phase was rich in H_2O, as indicated by the assemblages titanite + calcite + quartz and lawsonite + calcite, which require X_{CO_2} values less than 0·03 and 0·08, respectively. The P–T–X_{CO_2} conditions for the Queyras unit lie within the part of glaucophane + calcium carbonate stability field (Fig. 9) in which clinopyroxene is not stable. This is consistent with the assemblages reported by Ballèvre & Lagabrielle (1994).

The stability limits of glaucophane + aragonite shown in Figs 8 and 9 are best applied in the high-pressure range, where the assemblages and mineral compositions reflect those observed in thin sections. Low-pressure limits on glaucophane + aragonite may involve phases not included in our modelling and will almost certainly involve more complex solid solution models for amphiboles at the transition to lower pressure greenschist- or epidote–amphibolite-facies conditions. The slightly elevated calcium contents in the zoned glaucophane from sample A2C (Table 2) may be an indication of the necessity to consider glaucophane solid solution with Ca-amphibole end-members at lower pressures. We have chosen not to attempt to model rigorously the lower pressure reactions, as we have no phase assemblage evidence to guide the effort.

Other limits on *P*, *T* and fluid composition

The peak fluid X_{CO_2} compositions appear to be best constrained by mineral equilibria, although fluid inclusion studies by Barr (1990) and Moree (1998) did not detect CO_2 in fluids that were either post-peak metamorphic or could not be conclusively identified as peak metamorphic. In addition to glaucophane + calcite/aragonite, the other common assemblages dolomite + quartz and lawsonite + epidote constrain P, T and fluid composition on Syros. These assemblages suggest that fluids in both the marbles and in the various interlayered schist types must have been very rich in H_2O relative to CO_2. As noted above, this is consistent with the observations of Ballèvre & Lagabrielle (1994), who suggested X_{CO_2} values less than 0·03 and 0·08 based on the stability of two different observed assemblages in their Alpine rocks.

Several mineral assemblage common on Syros also constrain the maximum X_{CO_2} values in rocks interlayered with the glaucophane-bearing marbles. Dixon (1976), Ridley (1982*a*) and petrographic studies that accompanied the mapping of the northern half of Syros by students from the University of Freiburg, Germany (1996–2000) have shown that lawsonite + epidote is relatively common and

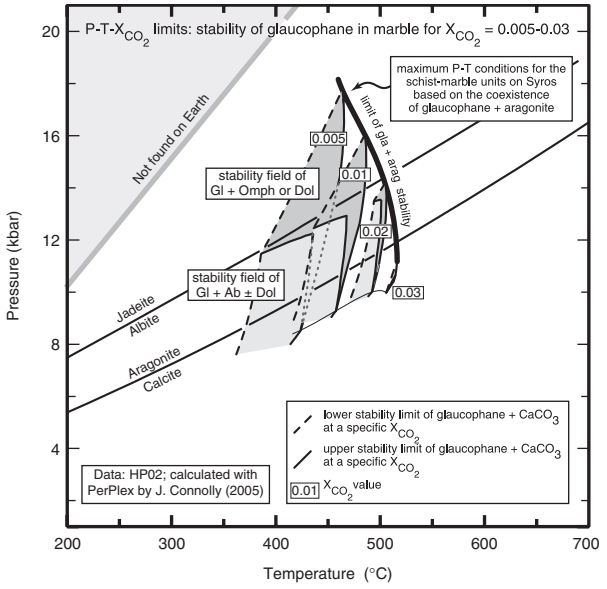

Fig. 9. Pressure vs temperature diagram that shows the limits of calcite/aragonite + glaucophane stability for four fluid compositions (X_{CO_2} = 0·005, 0·01, 0·02 and 0·03). Reactions are in the system $NaAlO_2$–CaO–MgO–SiO_2–H_2O–CO_2. The calculations were carried out using the same input parameters as in Fig. 8. The maximum P–T at the four fluid compositions traces a curve that represents the maximum possible stability of glaucophane + aragonite.

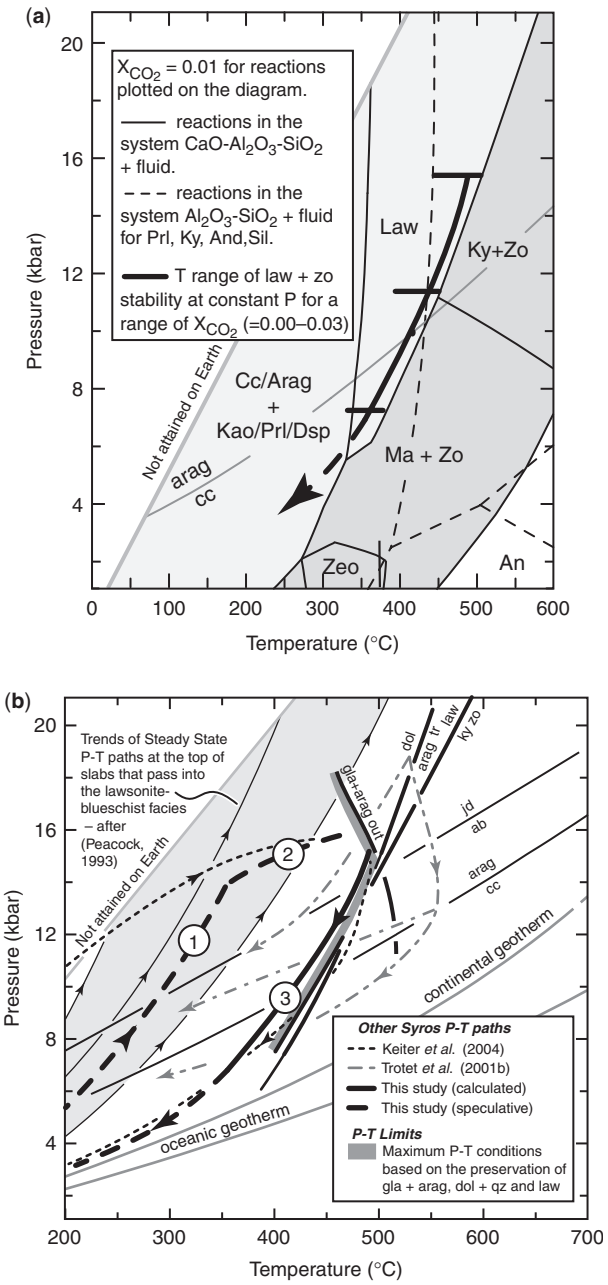

Fig. 10. Pressure vs temperature diagrams. (a) Reactions in the system CaO–Al_2O_3–SiO_2–H_2O–CO_2 that determine the limits on lawsonite stability. The bold black lines show the calculated range of temperatures over which lawsonite + zoisite (epidote) are stable at 15, 11 and 7 kbar. (b) A summary of the constraints, limits and inferences used to construct a P–T trajectory for the interlayered schist and marble units, and comparison of our best current estimate of a P–T trajectory with two paths from the literature. Numbered segments or legs of the P–T trajectory are referred to in the text. An, anorthite; arag, aragonite; cc, calcite; Dsp, diasphore; kao, kaolinite; Ky, kyanite; Ma, margarite; Law, lawsonite; Prl, pyrophyllite; Zeo, zeolites (all the Ca–Al in the database were used and grouped in this field), Zo, zoisite. Calculations were carried out as described in Fig. 8.

that the expected high-temperature breakdown products of lawsonite, such as kyanite + zoisite (epidote) or margarite + zoisite (epidote), are not present. Consequently, the reactions lawsonite = kyanite + zoisite + quartz + H_2O and lawsonite = margarite + zoisite + quartz + H_2O limit the maximum T at given P for the peak metamorphism and the retrograde P–T trajectory (Fig. 10a). The survival of lawsonite indicates that water-rich fluids (<3% CO_2) were common in the schists for much of the metamorphic history. In the system Na_2O–CaO–Al_2O_3–SiO_2–H_2O–CO_2, calculated T–X_{CO_2} stability of the assemblage lawsonite + zoisite (epidote) for a range of pressures shows that these two phases can coexist only over a narrow range of temperatures and with H_2O-rich fluids. For example, Fig. 11 shows that at 15 kbar, lawsonite + zoisite (epidote) coexist only at about 450–510°C at X_{CO_2} < 0·03, and Fig. 11 also shows a number of other observed assemblages that are all consistent with these water-rich fluids. Similar calculations were carried out at 11 and 7 kbar (not presented) for lawsonite + zoisite to help limit the retrograde P–T trajectory (Fig. 10a) that returned these rocks to the surface.

The assemblage dolomite + quartz is common in many of the marbles that lack a Na-rich phase. Because these marbles did not develop either tremolite or diopside, the implication is that temperatures did not exceed the stability of dolomite + quartz. The breakdown of dolomite + quartz to tremolite (X_{CO_2} = 0·01) has a steep P–T slope of about 9–10°C/kbar that limits the maximum temperature

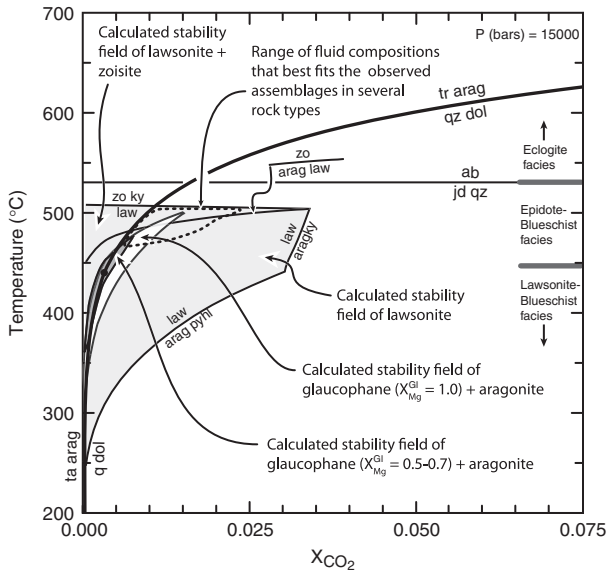

Fig. 11. Temperature vs X_{CO_2} diagram at 15 kbar that shows the stability limits for various assemblages: lawsonite (law) stability and lawsonite + zoisite (zo) stability in the system Na_2O–CaO–Al_2O_3–SiO_2–H_2O–CO_2, quartz (qz) + dolomite (dol) and glaucophane$_{ss}$ + aragonite (arag) from Fig. 8c. The temperature range of lawsonite + zoisite stability shown here and for similar diagrams constructed at 11 and 7 kbar is used to constrain the uplift path in Fig. 10a and b. Facies boundaries are after Evans (1990) and Peacock (1993). Calculations were carried out as described in Fig. 8. ab, albite; jd, jadeite; ky, kyanite; pyhl, pyrophyllite.

these rocks could have reached to about 475–560°C at about 13–21 kbar, respectively (Fig. 10b).

Limits placed on fluid composition by both lawsonite + epidote in the schists and glaucophane + aragonite/calcite in the marbles suggest that the attending metamorphic fluid phase was water-rich, although local internal buffering of the fluid composition cannot be completely excluded. However, because the stability of glaucophane requires water-rich fluids, the glaucophane-bearing parts of the marbles, at least, were probably open to pervasive fluid flow of an external H_2O-rich fluid. Had the grain-boundary fluid been internally buffered, any reaction of glaucophane + calcium carbonate, which produces a CO_2-rich fluid, should have led to the decomposition of the glaucophane. Additionally, experimental studies have suggested that the marble would be permeable only to an H_2O-fluid (Watson & Brenan, 1987; Brenan & Watson, 1988; Brenan, 1991; Holness, 1992; Holness & Graham, 1995). Such studies on calcite (and by analogy aragonite?) showed that increased CO_2 in the fluid increases the dihedral angle at the fluid–mineral interface, leading to the entrapment of fluid along the grain boundaries and rendering the marble units relatively impermeable; in contrast, a low CO_2 and elevated brine content has been shown to lower the dihedral angle (e.g. Watson & Brenan, 1987; Brenan, 1991; Lee *et al.*, 1991), which would allow grain-boundary flow. It is worth noting that the only fluid inclusion studies from Syros (Barr, 1990; Moree, 1998) have yielded fluids compositions that, in addition to being CO_2-free, are moderately saline—about 6–12 wt % equivalent NaCl, rarely >20 wt % equivalent NaCl. Although these inclusions are most probably retrograde, if these fluids were compositionally analogous to the attending fluid at peak metamorphic conditions, then their compositions correspond to those most likely to form an interconnecting grain-boundary fluid in the marble.

Deformation is another factor that could promote fluid flow into the glaucophane marbles. During deformation, migration of grain boundaries by either diffusion or dislocation would enhance reaction and diffusion rates (see Baxter & DePaolo, 2004, and references therein). The glaucophane marbles show the same principal foliation as the schists and clearly recystallized during the main fabric-forming deformation, which could have promoted fluid infiltration in the glaucophane marbles.

Modelling of the stability of key assemblages in both the glaucophane marbles and the associated mafic rocks, as well as inferences for fluid inclusion studies and experimental work on grain-boundary fluid in marbles, place general limits on P–T–X_{fluid} conditions experienced by these rocks. The schist–marble sequences that contain the glaucophane-bearing marbles limit the peak metamorphic temperatures within the epidote–blueschist facies to ≤515°C and peak metamorphic pressures to below about 17 kbar with fluid compositions of <0·03 X_{CO_2} in most rocks (Fig. 10b).

P–T trajectory

Figure 10b illustrates the construction of our preferred P–T trajectory. The concave-up portion of prograde path (leg 1, Fig. 10b) is suggested by the examples of steady-state P–T paths that pass into the lawsonite–blueschist stability field (Peacock, 1993). Pseudomorphs after lawsonite are abundant in the blueschists of Syros, and the subduction P–T trajectory must have entered the lawsonite–blueschist facies, where the rocks must have initially equilibrated. Reaching the conditions of the epidote–blueschist facies requires a perturbation of the steady-state P–T trajectory, and the essential component is heating at a higher rate (leg 2, Fig. 10). Attaining the conditions of the epidote–blueschist facies is marked, partly, by the end of the stability of glaucophane + lawsonite via the reaction glaucophane + lawsonite = clinozoisite + paragonite + chlorite + quartz + water (Evans, 1990).

Determining precise pressure and temperature maxima are more difficult. As discussed above, the stability of lawsonite + Al-rich epidote in glaucophane-free and glaucophane-poor bulk compositions, and the lack of terminal lawsonite breakdown assemblages such as kyanite + zoisite and margarite + zoisite strongly suggest that the P–T trajectory for the schist–marble units remained

largely within the lawsonite stability field (Fig. 10b). Similarly, the presence of dolomite + quartz and the lack of their higher temperature breakdown products calcite/aragonite + tremolite (Fig. 10b) also place a thermal maximum on the P–T trajectory of these rocks that nearly coincides with the position of the lawsonite-out reactions.

The assemblage glaucophane + calcite/aragonite provides an upper constraint on the pressure and temperature. For the range of fluid compositions ($X_{CO_2} = 0{\cdot}005$–$0{\cdot}030$) over which glaucophane + aragonite are stable, the upper pressure boundary is a locus of points that form a curved, concave-downward line with a negative slope. For $X_{CO_2} = 0{\cdot}01$ the maximum pressure at which glaucophane + calcite/aragonite could remain stable would be just under 16 kbar at about 480°C (Figs 9 and 10a); the maximum temperature would be at 15 kbar just above 500°C. These estimates limit the maximum P–T conditions of the schist–marble sequence.

The initial leg of the retrograde P–T trajectory (leg 3, Fig. 10b) is constrained by the relict lawsonite + epidote assemblages that are found in the schists (Figs 10 and 11). For pure H_2O fluids, lawsonite + zoisite are stable from about 510 to 450°C, but this range shrinks and terminates at just above 500°C as X_{CO_2} approaches 0·03 (Fig. 11). At low temperatures (<300°C), both the oceanic and continental geotherms converge, and it is reasonable that the P–T trajectory of the marbles and schists would also approach these geotherms near the end of exhumation, as there are no locally observed late events on Syros that have the potential to disturb the geotherm (Fig. 10b).

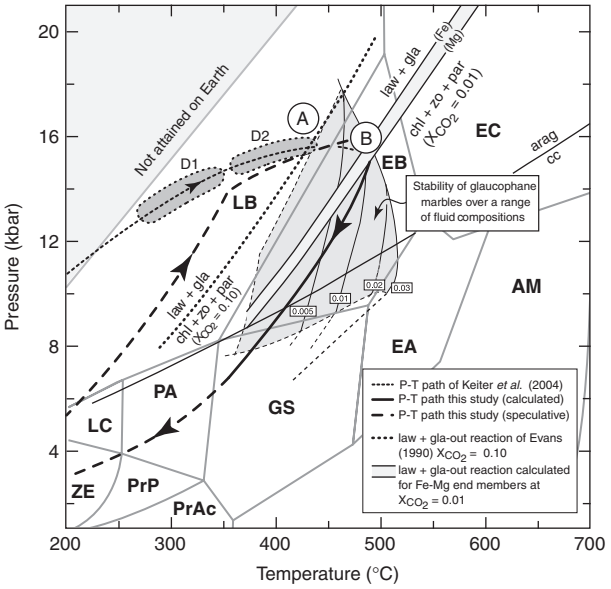

Fig. 12. Pressure vs temperature diagram that illustrates the petrological constraints on stages of the tectonic fabric development and the effect of X_{CO_2} on the P–T conditions of these constraints. Grey fields along the P–T path that are labelled D_1 and D_2 are estimates of the conditions of prograde deformation after Keiter *et al.* (2004); upper P–T conditions of D_2, the main fabric-forming event, are limited by the reaction glaucophane (gla) + lawsonite (law) = chlorite (chl) + zoisite (zo) + paragonite (par). Facies: AM, amphibolite; EA, epidote–amphibolite; EB, epidote–blueschist; EC, eclogite; GS, greenschist; LB, lawsonite blueschist; LC, lawsonite–chlorite; PA, pumpellyite–actinolite; PrAc, prehnite–actinolite; PrP, prehnite–pumpellyite; ZE, zeolite (Peacock, 1993). The letters A and B inside circles show two sets of P–T conditions at which some lawsonite pseudomorphs could have formed (see text for discussion on the relationship of some lawsonite pseudomorphs to the timing of the main D_2 foliation).

DISCUSSION

Metamorphism and the tectonic fabric

Rosenbaum *et al.* (2002) estimated that the main deformation and fabric-forming event (D_2) on Syros occurred at or near peak metamorphic conditions, which were loosely defined by them within the range of 400–520°C and 11–15 kbar with a peak at about 490°C and 15·2 kbar (Rosenbaum *et al.*, 2002, fig. 9). In contrast, Keiter *et al.* (2004) have reasoned that the main fabric-forming deformation (also D_2) was completed before the thermal peak of metamorphism. Keiter *et al.* (2004) based their conclusion on the observation that pseudomorphs of lawsonite commonly preserve traces of the D_2 fabric (main penetrative deformation). Keiter *et al.* (2004) suggested that this fabric would not survive if deformation occurred after a pseudomorph-forming reaction such as glaucophane + lawsonite = clinozoisite + paragonite + chlorite + quartz + water (one of several possible lawsonite–glaucophane-out reactions). Keiter *et al.* (2004, fig. 13) used the P–T position of a lawsonite–glaucophane-out reaction that was given in Evans (1990) as the upper thermal limit for penetrative deformation (location A in Fig. 12). Although we concur with Keiter *et al.* (2004) that inclusion trails in lawsonite pseudomorphs would probably not survive penetrative deformation that postdates the formation of the pseudomorph, we find it difficult to reconcile widespread glaucophane marbles with their P–T–t–d relations. The glaucophane marbles show the same D_2 fabric that is preserved in the lawsonite pseudomorphs, but our calculations show that the lower thermal stability of glaucophane + aragonite would have only just been reached when deformation ceased (based on their timing), even if the attending fluid was nearly pure H_2O (location A in Fig. 12). If these H_2O-rich fluid compositions ($X_{CO_2} \leq 0{\cdot}005$) are externally buffered, then glaucophane in foliated marbles should have broken down before peak metamorphic conditions were reached, and any glaucophane that would have formed in marbles with slightly higher X_{CO_2} fluids (0·01–0·03) should not be aligned in the D_2 fabric (P–T of location A in Fig. 12). This is contrary to observations from numerous localities.

The key to resolving the conflicting relative P–T–t–d conditions inferred from the lawsonite pseudomorphs (Keiter *et al.*, 2004) and those suggested by both

Rosenbaum *et al.* (2002) and the glaucophane-bearing marbles from this study, lies in remembering that Evans (1990) used an X_{CO_2} value of 0·10 for his H_2O-rich calculations. Evans (1990) demonstrated that the *P*–*T* locations of all the blueschist-facies reactions, including the lawsonite-out reaction used by Keiter *et al.* (2004), are highly dependent on the X_{CO_2} of the fluid. Following the lead of Evans (1990), we believe that the lawsonite-out reaction in question would be located at higher *T* because common assemblages from both the marbles and the associated schists suggest that the pervasive fluids were richer in water ($X_{CO_2} < 0{\cdot}03$, and probably $X_{CO_2} \cong 0{\cdot}01$). This would push the lawsonite–glaucophane-out reaction that is in question to higher temperatures by about 60°C, and it would lie at about 500°C (*P*–*T* of location B in Fig. 12). As a result, the main penetrative deformation on Syros could easily have occurred penecontemporaneously with peak metamorphism. The lawsonite pseudomorphs with the inclusion trails that were discussed by Keiter *et al.* (2004) could have formed during the initial decompression of the terrain. This shift of the lawsonite–glaucophane-out reaction to higher temperature as a result of the lower X_{CO_2} reconciles the *P*–*T* conditions of D_2 proposed by Keiter *et al.* (2004) with those of Rosenbaum *et al.* (2002). These conditions of *P*–*T*–deformation and the uplift *P*–*T* trajectory are also consistent with the observations and interpretations of Brady *et al.* (2004) that aragonite that is now seen only as pseudomorphs coarsened after the main deformation.

Other *P*–*T* trajectories

Until recently, most workers have placed the peak of metamorphism on both Syros and Sifnos near 15–16 kbar and 500°C (see Schliestedt, 1986; Dixon & Ridley, 1987; Okrusch & Bröcker, 1990; Avigad & Garfunkel, 1991; Rosenbaum *et al.*, 2002; Schmädicke & Will, 2003; Keiter *et al.*, 2004; Putlitz *et al.*, 2005; Fig. 12 of the present study). Many of these *P*–*T* paths are not well constrained, and several of these paths are stated to be schematic (e.g. Rosenbaum *et al.*, 2002; Keiter *et al.*, 2004). The work of Trotet *et al.* (2001*b*) was more detailed, and their result differed significantly from earlier attempts to construct a *P*–*T* trajectory for Syros. Trotet *et al.* (2001*b*) estimated peak conditions to be about 19 kbar and 525°C, using some of their own activity models, the TWEEQU method (Berman, 1991) and the Berman JUN02 data. Trotet *et al.* (2001) also constructed multiple retrograde paths for both Syros and Sifnos (Fig. 10b). Parts of these *P*–*T* paths suggested by Trotet *et al.* (2001*b*) diverge significantly from the estimates in our study and many of the others cited above. In particular, we find it difficult to reconcile those parts of the *P*–*T* paths of Trotet *et al.* (2001*a*, 2001*b*) that significantly exceed the upper stability limits of both lawsonite and dolomite + quartz (Fig. 10b), both of which are widely distributed in the schists and marbles across Syros. A full analysis of the work of Trotet *et al.* (2001*b*) is beyond the scope of this study, but we point out that TWEEQU pressure–temperature intersections, even tightly clustered ones, do not guarantee the accuracy of the estimate. Berman (1991, fig. 5c) showed that the same data can yield diverse *P*–*T* locations through the choice of different activity models for a single phase. Additionally, Cooke *et al.* (2000, figs 14 and 15) showed two sets of tight intersections at widely divergent *P*–*T* locations that were obtained for the same set of TWEEQU equilibria through minor reinterpretation of equilibrium assemblages and choice of mineral compositions. As a consequence, we feel that the limits imposed by net-transfer equilibria, such as those cited in this study, can give a better picture of the *P*–*T* evolution of the schist–marble sequences.

Other *P*–*T* maxima and their interpretation

The work of Trotet *et al.* (2001*b*) has also provided some of the earliest evidence that rocks from the mafic–ultramafic unit on Syros and Sifnos might have attained higher peak metamorphic conditions (about 19 kbar and 525°C for Syros and about 19 kbar and 580°C for Sifnos). Schmädicke & Will (2003) also suggested higher peak metamorphic conditions of about 19 kbar and 570°C for Sifnos. In recent work, Gitahi (2004), Holly (2004) and Holly *et al.* (2004) applied the geothermobarometer of Ravna & Terry (2004) to minerals from the eclogitic 'knockers' of the the mafic–ultramafic unit on Syros. Their work suggested that conditions could range as high as 19–24 kbar (±2 kbar) at temperatures of 500–580°C (±65°C). These estimates considerably exceed the conditions at which glaucophane + aragonite are stable, but a possible explanation is that the mafic–ultramafic sequences, which are separated from the schist, marble and blueschist units by tectonic boundaries, had a different early *P*–*T* history. The fabric suggests that all the rocks on Syros experienced the same penetrative deformation, so if the early *P*–*T* histories differed, then the whole package must have been assembled by the time of the main deformation, D_2 of Rosenbaum *et al.* (2002) and Keiter *et al.* (2004). A plausible (but not the only) scenario could be as follows.

(1) The mafic and ultramafic rocks, already metamorphosed at eclogite-facies conditions, were attached to the upper plate earlier and underwent uplift.

(2) At or near 15 kbar and 500°C the slices of the schist and marble units were sheared off the down-going plate and became juxtaposed with mafic and ultramafic rocks in the upper plate. The process of assembling the package of rocks that crop out on Syros at present would have marked the main deformational and fabric-forming event. This deformation and metamorphism could have pervasively overprinted the matrix containing and the margins of the eclogitic 'knockers' that preserve evidence of the higher *P*–*T* conditions; however, for the schist and marble

sequences, these conditions would represent the peak metamorphism.

(3) Following the main deformation and metamorphism, the whole package of rocks could have begun its exhumation cycle. During the exhumation phase, episodic hydration, minor open folding, local crenulation or chevron-style folding and fracturing occurred; however, no penetrative fabric developed and there was mostly only local deformation of the main fabric. Within the marbles, widespread preservation of calcite pseudomorphs after aragonite supports the view that no pervasive deformation subsequent to the main D_2 event occurred. However, the marbles also show late, localized planes of shearing that appears to have affected the aragonite, which coarsened after the main D_2 event, rather than the calcite of the pseudomorph (see Brady *et al.*, 2004, fig. 6).

CONCLUSIONS

On Syros, glaucophane + aragonite/calcite is common in impure marble precursors that were probably admixtures of calcium carbonate and mafic igneous material. Stability of glaucophane + aragonite/calcite is restricted to a pressure–temperature range of about 8–17 kbar and about 350°C to just above 500°C depending upon the grain-boundary fluid composition, which must have X_{CO_2} less than about 0·03. These impure marble bulk compositions would contain albite or jadeite ± dolomite at P and T conditions below glaucophane + aragonite/calcite stability and omphacite ± dolomite at P and T conditions above glaucophane + aragonite/calcite stability.

The occurrence of glaucophane + aragonite/calcite is a petrological indicator. The assemblage places limits on both the maximum and minimum P–T conditions of formation. On Syros, glaucophane from the marbles is aligned with the main tectonic fabric, strongly suggesting that the main deformational phase occurred within the stability field of the assemblage glaucophane + aragonite, probably at about 15 kbar and about 500°C. Glaucophane + aragonite/calcite is a monitor of fluid composition, and calculations indicate that glaucophane + Ca-carbonate is stable only in water-rich fluids ($X_{CO_2} < 0{\cdot}03$). The necessity of having an impure carbonate bulk composition that equilibrates in a restricted P–T–X_{CO_2} stability field within a subduction setting probably explains the scarcity of reported glaucophane-bearing marbles.

On Syros, the glaucophane-bearing marbles and the presence of relict lawsonite + epidote both support the existence of a widespread, water-rich grain-boundary fluid ($X_{CO_2} < 0{\cdot}03$). These fluids probably had X_{CO_2} values closer to 0·01. The scale of preservation of the glaucophane marbles and the lawsonite suggests that, on Syros, it was likely that an H_2O-rich fluid was present in the marble–schist units over much of their metamorphic history. The presence of a water-rich grain-boundary fluid in carbonate-rich rocks that appears to have been maintained over a wide range of P–T conditions is one of the more surprising results of this study.

ACKNOWLEDGEMENTS

The authors thank the Keck Geology Consortium, which funded some of this research. J.C.S. also thanks the Deutsche Forschungsgemeinschaft for past support (Schu 919/6-1). We offer thanks to Michael Raith and John Ridley for reviews that improved the manuscript. J.C.S. also thanks Stuart Kearns, the master of beam technology at Bristol. We would like to acknowledge the wonderful hospitality of the people of Syros. We were welcomed as friends and treated as relatives. We especially want to thank Mr Georgios Rigoutsos and his family, the proprietors of the Hotel Olympia in Finikas, our home on Syros. Georgios with his friendly advice and knowledge of the island made our visits most pleasurable, leaving us with only the fondest of memories and a desire to return. We are also grateful to Nikos Printezis, the Captain of the *Perla I*, which transported us to and retrieved us from numerous rocky points and beaches all around northern Syros.

REFERENCES

Altherr, R., Schliestedt, M., Okrusch, M., Seidel, E., Kreuzer, H., Harre, W., Lenz, H., Wendt, I. & Wagner, G. A. (1979). Geochronology of high-pressure rocks on Sifnos (Cyclades, Greece). *Contributions to Mineralogy and Petrology* **70**, 245–255.

Anderissen, P. A. M., Boelrijk, N. A. I. M., Hebeda, E. H., Priem, H. N. A., Verdurmen, E. A. Th. & Verschure, R. H. (1979). Dating the events of metamorphism and granitic magmatism in the Alpine orogen of Naxos (Cyclades, Greece). *Contributions to Mineralogy and Petrology* **69**, 215–225.

Avigad, D. & Garfunkel, Z. (1989). Low-angle faults above and below a blueschist belt: Tinos Island, Cyclades, Greece. *Terra Nova* **1**, 182–187.

Avigad, D. & Garfunkel, Z. (1991). Uplift and exhumation of high-pressure metamorphic terrains: the example of the Cycladic blueschist belt (Aegean Sea). *Tectonophysics* **188**, 357–372.

Ballèvre, M. & Lagabrielle, Y. (1994). Garnet in blueschist-facies marbles from the Queyras Unit (Western Alps)—Its occurrence and its significance. *Schweizerische Mineralogisch-Petrographische Mitteilung* **74**, 203–212.

Barr, H. (1990). Preliminary fluid inclusion studies in high-grade blueschist terrain, Syros, Greece. *Mineralogical Magazine* **54**, 159–168.

Baxter, E. F. & DePaolo, D. J. (2004). Can metamorphic reactions proceed faster than bulk strain? *Contributions to Mineralogy and Petrology* **146**, 657–670.

Berman, R. G. (1991). Thermometry using multi-equilibrium calculations: a new technique, with petrological applications. *Canadian Mineralogist* **29**, 833–855.

Boundy, T. M., Donohue, C. L., Essene, E. J., Mezger, K. & Austrheim, H. (2002). Discovery of eclogite facies carbonate rocks from the Lindas Nappe, Caledonides, Western Norway. *Journal of Metamorphic Geology* **20**, 649–667.

Brady, J. B., Markley, M. J., Schumacher, J. C., Cheney, J. T. & Bianciardi, G. A. (2004). Aragonite pseudomorphs in high-pressure marbles of Syros, Greece. *Journal of Structural Geology* **26**, 3–9.

Brenan, J. M. (1991). Development and maintenance of metamorphic permeability: implications for fluid transport processes. In: Kerrick, D. M. (ed.) *Contact Metamorphism. Mineralogical Society of America, Reviews in Mineralogy* **26**, 291–315.

Brenan, J. M. & Watson, E. B. (1988). Fluids in the lithosphere 2. Experimental constraints on CO_2 transport in dunite and quartzite at elevated P–T conditions with implications for mantle and crustal decarbonation processes. *Earth and Planetary Science Letters* **91**, 141–158.

Bröcker, M. & Enders, M. (1999). U–Pb zircon geochronology of unusual eclogite-facies rocks from Syros and Tinos (Cyclades, Greece). *Geological Magazine* **136**, 101–118.

Bröcker, M., Kreuzer, H., Matthews, A. & Okrusch, M. (1993). $^{40}Ar/^{39}Ar$ and oxygen isotope studies of polymetamorphism from Tinos island, Cycladic blueschist belt, Greece. *Journal of Metamorphic Geology* **11**, 223–240.

Castelli, D. (1991). Eclogitic metamorphism in carbonate rocks—the example of impure marbles from the Sesia–Lanzo Zone, Italian Western Alps. *Journal of Metamorphic Geology* **9**, 61–77.

Cheney, J. T., Schumacher, J. C., Coath, C. D. *et al.* (2000). Ion microprobe ages of zircons from blueschists, Syros, Greece. *Geological Society of America Abstracts with Programs* **32**, A152.

Connolly, J. A. D. (1990). Multivariable phase-diagrams—an algorithm based on generalized thermodynamics. *American Journal of Science* **290**, 666–718.

Connolly, J. A. D. (2005). Computation of phase equilibria by linear programming: A tool for geodynamic modeling and its application to subduction zone decarbonation. *Earth and Planetary Science Letters* **236**, 524–541.

Cooke, R. A., O'Brien, P. J. & Carswell, D. A. (2000). Garnet zoning and the identification of equilibrium mineral compositions in high-pressure–temperature granulites from the Moldanubian Zone, Austria. *Journal of Metamorphic Geology* **18**, 551–569.

Dale, J., Holland, T. & Powell, R. (2000). Hornblende–garnet–plagioclase thermobarometry: a natural assemblage calibration of the thermodynamics of hornblende. *Contributions to Mineralogy and Petrology* **140**, 353–362.

Dixon, J. E. (1976). Glaucophane schists of Syros, Greece (abstract). *Bulletin de la Société Géologique de France* **18**, 280.

Dixon, J. E. & Ridley, J. (1987). Syros. In: Helgeson, H. C. (ed.) *Chemical Transport in Metasomatic Processes*. Dordrecht: D. Reidel, pp. 489–518.

Evans, B.W. (1990). Phase relations of epidote-blueschists. *Lithos* **25**, 3–23.

Frey, M. (1987). Very low-grade metamorphism of clastic sedimentary rocks. In: Frey, M. (ed.) *Low Temperature Metamorphism*. Glasgow: Blackie, pp. 9–58.

Gitahi, N. (2004). Geochemistry and metamorphic evolution of eclogites on Syros island, Greece. Extended Abstracts, Seventeenth Annual Keck Research Symposium in Geology Proceedings, Lexington, VA, P.81-4. Available at <http://www.science.smith.edu/departments/Geology/Greece/Abstracts/Nwgitahi_Abs.pdf>

Hecht, J. (1984). *Geological map of Greece 1:50 000, Syros island*. Athens: Institute of Geology and Mineral Exploration.

Holland, T. J. B. & Powell, R. (1996). Thermodynamics of order–disorder in minerals; II, Symmetric formalism applied to solid solutions. *American Mineralogist* **81**, 1425–1437.

Holland, T. J. B. & Powell, R. (1998). An internally consistent thermodynamic data set for phases of petrological interest. *Journal of Metamorphic Geology* **16**, 309–343.

Holly, E. A. (2004). Pressure–temperature conditions of metamorphism in eclogites, Syros, Greece, Extended Abstracts, Seventeenth Annual Keck Research Symposium in Geology Proceedings, Lexington, VA, P.81-84. Available at <http://www.science.smith.edu/departments/Geology/Greece/Abstracts/Holley_Abs.pdf>

Holly, E. A., Ross, T. & Cheney, J. T. (2004). Pressure–temperature conditions of metamorphism in eclogites, Syros, Greece. *Geological Society of America, Abstracts with Programs* **36**(1), A67.

Holness, M. B. (1992). Equilibrium dihedral angles in the system quartz–CO_2–H_2O–NaCl at 800°C and 1–15 kbar: the effects of pressure and fluid composition on the permeability of quartzites. *Earth and Planetary Science Letters* **114**, 171–184.

Holness, M. B. & Graham, C. M. (1995). *P–T–X* effects on equilibrium carbonate–H_2O–CO_2–NaCl dihedral angles: constraints on carbonate permeability and the role of deformation during fluid infiltration. *Contributions to Mineralogy and Petrology* **119**, 301–313.

Keiter, M., Piepjohn, K., Ballhaus, C., Bode, M. & Lagos, M. (2004). Structural development of high-pressure metamorphic rocks on Syros island (Cyclades, Greece). *Journal of Structural Geology* **26**, 1433–1445.

Kenter, J. A. M. (1990). Carbonate platform flanks: slope angle and sediment fabric. *Sedimentology* **37**, 777–794.

Kerrick, D. M. & Jacobs, G. K. (1981). A modified Redlich–Kwong equation for H_2O, CO_2, H_2O–CO_2 mixtures at elevated pressures and temperatures. *American Journal of Science* **281**, 735–767.

Korzhinskii, D. S. (1959). *Physiochemical Basis of the Analysis of the Petrogenesis of Minerals*. New York: Consultants Bureau.

Leake, B. E., Woolley, A. R., Arps, C. E. S. *et al.* (1997). Nomenclature of amphiboles: Report of the Subcommittee on Amphiboles of the International Mineralogical Association, Commission on New Minerals and Mineral Names. *American Mineralogist* **82**, 1019–1037.

Lee, V. W., Mackwell, S. J. & Brantley, S. L. (1991). The effect of fluid chemistry on wetting textures in ovaculite. *Journal of Geophysical Research* **96**, 10023–10037.

Moree, M. (1998). The behavior of retrograde fluids in high-pressure settings. Ph.D. thesis, Vrije Universiteit Amsterdam, 162 pp.

Morimoto, N., Fabries, J., Ferguson, A. K., Ginzburg, I. V., Ross, M., Deifert, F., Zussman, J., Aoki, K. & Gottardi, G. (1988). Nomenclature of pyroxenes. *Mineralogical Magazine* **52**, 535–550.

Nitsch, K.-H. (1972). Das *P–T–*X_{CO_2}–Stabilitätsfeld von Lawsonit. *Contributions to Mineralogy and Petrology* **34**, 116–134.

Okrusch, M. & Bröcker, M. (1990). Eclogites associated with high-grade blueschists in the Cyclades archipelago, Greece: a review. *European Journal of Mineralogy* **2**, 451–478.

Peacock, S. M. (1993). The importance of blueschist–eclogite dehydration reactions in subducting crust. *Geological Society of America Bulletin* **105**, 684–694.

Pohl, J. (1999). Geologie und Hochdruckgesteine der Insel Syros, Griechenland. Diploma thesis, Geologisches Institut, Albert-Ludwigs Universität, Freiburg, 107 pp.

Putlitz, B., Cosca, M. A. & Schumacher, J. C. (2005). Prograde mica $^{40}Ar/^{39}Ar$ growth ages recorded in high pressure rocks (Syros, Cyclades, Greece). *Chemical Geology* **214**, 79–98.

Ravna, E. J. K. & Terry, M. P. (2004). Geothermobarometry of UHP and HP eclogites and schists—an evaluation of equilibria among garnet–clinopyroxene–kyanite–phengite–coesite/quartz. *Journal of Metamorphic Geology* **22**, 579–592.

Ridley, J. (1981). Strain history and microfabrics in a blueschist terrain, Syros, Greece. *Journal of Structural Geology* **3**, 338.

Ridley, J. (1982*a*). *Tectonic style, strain history and fabric development in a blueschist terrain*, Syros, Greece. Ph.D. thesis, Edinburgh University, 283 pp.

Ridley, J. (1982*b*). Arcuate lineation trends in a deep level, ductile thrust belt, Syros, Greece. *Tectonophysics* **88**, 347–360.

Ridley, J. (1984*a*). Evidence of a temperature-dependent 'blueschist' to 'eclogite' transformation in high-pressure metamorphism of metabasic rocks. *Journal of Petrology* **25**, 852–870.

Ridley, J. (1984*b*). The significance of deformation associated with blueschist facies metamorphism on the Aegean island of Syros. In: Dixon, J. E. & Robertson, A. H. F. (eds) *The Geological Evolution of the Eastern Mediterranean. Geological Society, London, Special Publications* **17**, 545–550.

Ridley, J. (1984*c*). Listric normal faulting and the reconstruction of the synmetamorphic structural pile of the Cyclades. In: Dixon, J. E. & Robertson, A. H. F. (eds) *The Geological Evolution of the Eastern Mediterranean. Geological Society, London, Special Publications* **17**, 755–761.

Ridley, J. (1986). Parallel stretching lineations and fold axes oblique to a shear displacement direction—a model and observations. *Journal of Structural Geology* **8**, 647–653.

Robinson, P., Spear, F. S., Schumacher, J. C., Laird, J., Klein, C., Evans, B. W. & Doolan, B. L. (1982). Phase relations of metamorphic amphiboles: Natural occurrence and theory. In: Veblen, D. R. & Ribbe, P. H. (eds) *Amphiboles: Petrology and Experimental Phase Relations. Mineralogical Society of America, Reviews in Mineralogy* **9B**, 1–227.

Rosenbaum, G., Avigad, D. & Sanchez-Gomez, M. (2002). Coaxial flattening at deep levels of orogenic belts: evidence from blueschists and eclogites on Syros and Sifnos (Cyclades, Greece). *Journal of Structural Geology* **24**, 1451–1462.

Schliestedt, M. (1986). Eclogite–blueschist relationships evident by mineral equilibria in the high-pressure metabasic rocks of Sifnos (Cycladic islands), Greece. *Journal of Petrology* **27**, 1437–1459.

Schmädicke, E. & Will, T. M. (2003). Pressure–temperature evolution of blueschist facies rocks from Sifnos, Greece, and implications for the exhumation of high-pressure rocks in the Central Aegean. *Journal of Metamorphic Geology* **21**, 799–811.

Tomaschek, F. & Ballhaus, C. (1999). The Vari Unit on Syros (Aegean Sea) and its relation to the Attic–Cycladic Crystalline Complex. *Journal of Conference Abstracts* **4**, 72.

Tomaschek, F., Kennedy, A. K., Villa, I. M., Lagos, M. & Ballhaus, C. (2003). Zircons from Syros, Cyclades, Greece—Recrystallization and mobilization of zircon during high-pressure metamorphism. *Journal of Petrology* **44**, 1977–2002.

Trotet, F., Jolivet, L. & Vidal, O. (2001*a*). Tectono-metamorphic evolution of Syros and Sifnos islands (Cyclades, Greece). *Tectonophysics* **338**, 179–206.

Trotet, F., Vidal, O. & Jolivet, L. (2001*b*). Exhumation of Syros and Sifnos metamorphic rocks (Cyclades, Greece). New constraints on the *P–T* paths. *European Journal of Mineralogy* **13**, 901–920.

Wang, X. M. & Liou, J. G. (1993). Ultra-high-pressure metamorphism of carbonate rocks in the Dabie Mountains, Central China. *Journal of Metamorphic Geology* **11**, 575–588.

Watson, B. & Brenan, J. M. (1987). Fluids in the lithosphere, 1. Experimentally determined wetting characteristics of CO_2–H_2O fluids and their implications for fluid transport, host-rock physical properties, and fluid inclusion formation. *Earth and Planetary Science Letters* **85**, 497–515.

Wijbrans, J. R., Schliestedt, M. & York, D. (1990). Single grain argon laser probe dating of phengites from blueschist to greenschist transition of Sifnos (Cyclades, Greece). *Contributions to Mineralogy and Petrology* **104**, 582–593.

Ye, K. & Hirajima, T. (1996). High-pressure marble at Yangguantun, Rongcheng county, Shandong province, eastern China. *Mineralogy and Petrology* **57**, 151–165.